AD-A271 999

Remote Sensing of Crevice Corrosion

Phase I Final Report
Under ONR Contract No. N00014-93-C-0066

Submitted by:

Faraday Technology Inc
3155 Research Blvd., #105
Dayton, OH 45420-4011

Submitted to:

Dr. John A. Sedriks, Scientific Officer
Code 3310
Office of Naval Research
800 N. Quincy St.
Arlington, VA 22217-5660

October 1993

93-26037

93 10 26 073

Remote Sensing of Crevice Corrosion

Phase I Final Report
Under ONR Contract No. N00014-93-C-0066

Mahendra Sunkara, Ph.D. and Earl Jennings Taylor, Ph.D.

Faraday Technology Inc
3155 Research Blvd., #105
Dayton, OH 45420-4011

and

(under NCRADA-USNA-93-002)

Professor Patrick J. Moran
Department of Mechanical Engineering
United States Naval Academy
Annapolis, MD 21402

October 1993

Accesion For

NTIS	CRA&I	
DTIC	TAB	
Unannounced		
Justification		

By
Distribution

Availability Codes

| Dist | Avail and/or Special |

A-1

TABLE OF CONTENTS

1.0 EXECUTIVE SUMMARY

In the Phase I SBIR program entitled "Remote Sensing of Crevice Corrosion", we demonstrated the feasibility of an electrochemical/magnetic field technique for detecting crevice corrosion. Crevice corrosion is a form of localized corrosion that occurs within crevices or at shielded surfaces where stagnant solution is present. Crevice corrosion is particularly problematic for the Navy in networks of seawater piping where the numerous gasketed junctions are susceptible to crevice corrosion. Since the crevice corrosion is almost always confined to within the crevice itself, the pipe joints must be periodically disassembled and visually inspected for crevice corrosion. This process is tedious, time consuming, expensive, and subjective.

Based on the mechanistic aspects of crevice corrosion, we proposed and investigated several novel approaches for remote sensing of crevice corrosion. The key question defined in our Phase I proposal was

"Are any of these techniques sensitive enough to detect wether crevice corrosion is occuring or has occured?"

The Phase I program demonstrated an affirmative answer to this question.

Our approach to remote sensing of crevice corrosion is based on the fact that at low frequencies the low impedance of a crevice site relative to the high impedance passive film of the piping material. Our procedure involves the following steps

1) Exciting the crevice site with an AC current signal,
2) Generating enhanced current leakage through the low impedance crevice sites,
3) Detecting the crevice via the AC magnetic field associated with the enhanced leakage current.

In Figure E.1, we present data demonstrating the sensitivity of the AC magnetic field measurement of currents. These data were obtained at a frequency of 10 Hz and indicate a measurement sensitivity of $20\mu A/cm^2$. This sensitivity is more than adequate to measure the currents reported for crevice corrosion, specifically, $100\mu A/cm^2$.

In Figure E.2, we present data for the magnetic field measurement of a sample of SS 304 with and without a crevice site. The crevice site was formed from tightly fitting gaskets at the 9 inch position. In the absence of the crevice site, our magnetic field response is flat, indicating uniform leaking of the AC excitation signal. However, in the presence of a crevice corrosion site, we observe an enhanced magnetic field signal of 1.8X at the crevice corrosion site. The magnetic field signal was also enhanced beyond the crevice site due to the presence of additional low impedance pitting corrosion sites. The presence of crevice corrosion and of pitting corrosion was confirmed by subsequent visual inspection of the samples.
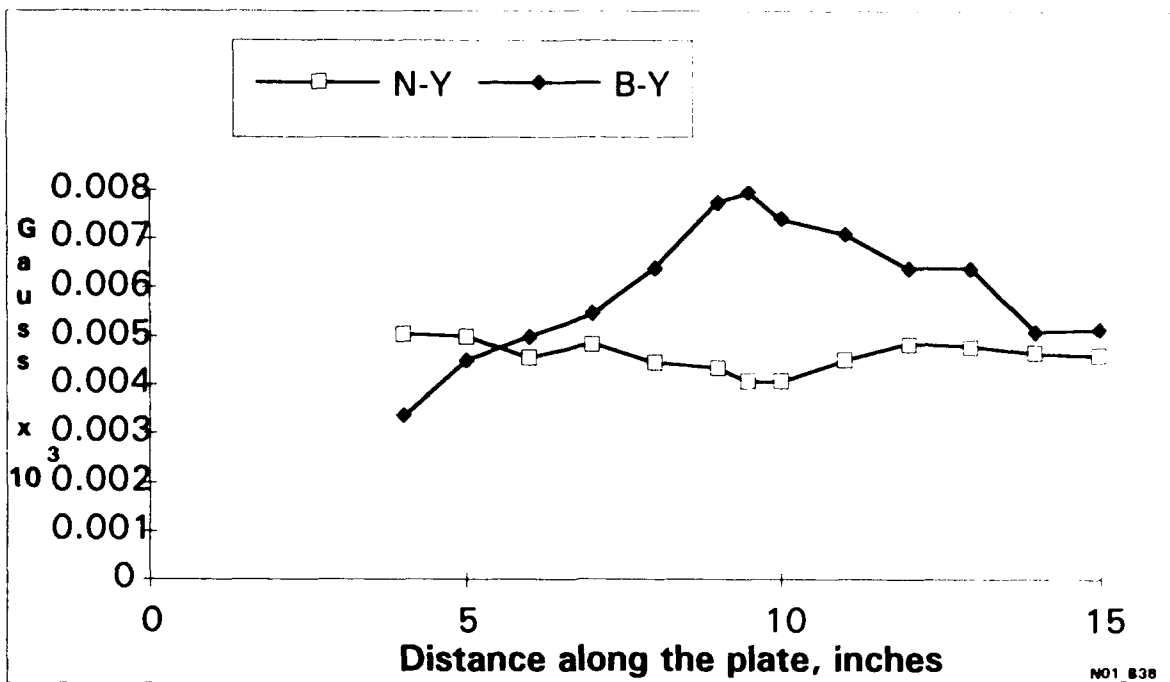
Figure E.1: Magnetic field measurements over crevice sites formed on a SS 304 steel by gaskets. Data from a SS-304 plate with no crevices is also shown.
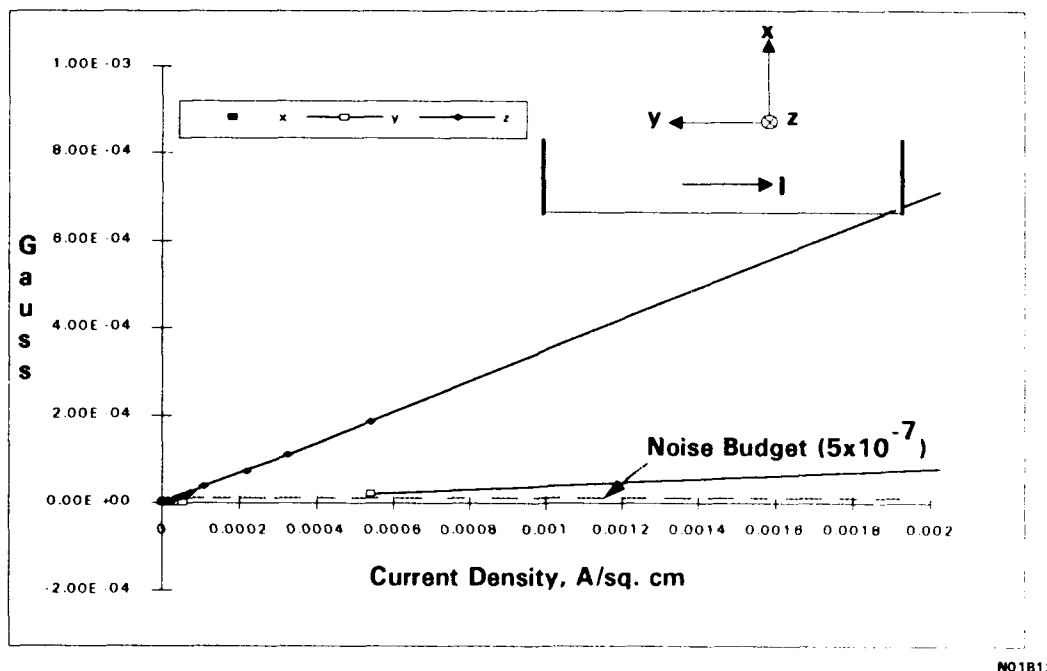

Figure E.2: AC sensitivity measurements with ionic flow in the calibration cell.

4

Based on these data, we envision a simple diagnostic procedure for the detection of crevice corrosion. The diagnostic would involve A.C. excitation of a piping system with multiple pipe joints and potential crevice corrosion sites. The magnitude of the magnetic field response would be criterion indicating crevice corrosion. By detecting the crevice corrosion in this "remote" manner, we would eliminate the time, cost, and uncertaintity associated with disassembly and visual inspection of each and every pipe joint.

2.0 SIGNIFICANCE OF THE PROBLEM

In the program "Remote Sensing of Crevice Corrosion," we proposed to demonstrate the feasibility of developing a diagnostic procedure for detecting crevice corrosion. Crevice corrosion is a form of localized corrosion that occurs within crevices or at shielded surfaces where stagnant solution is present. Crevice corrosion is particularly problematic for the Navy in networks of sea water piping where the numerous gasketed junctions are susceptible to crevice corrosion. Since the crevice corrosion is almost always confined to within the crevice itself, the pipe joints must be periodically disassembled and visually inspected for evidence of crevice corrosion. Visual inspection is time consuming, tedious, expensive, and subjective.

Alloy 625 was utilized as one of the primary piping materials in construction of the U.S. Navy's new Sea wolf submarine and a possible candidate for piping systems in future submarines. Alloy 625 exhibits excellent uniform corrosion and pitting corrosion resistance, excellent mechanical properties, and excellent weldability. However, Alloy 625 is susceptible to crevice corrosion in natural sea water. Furthermore, since Alloy 625 is not inherently resistant to biofouling in the marine environment, some form of biofouling control is required. Typically chlorination is employed to prevent biofouling. However, the crevice corrosion problem of Alloy 625 is exacerbated in chlorinated sea water [Moran, 1986].

In phase 1 program, we proposed three novel remote sensing concepts for crevice corrosion. These concepts were derived from an understanding of the mechanistic aspects of crevice corrosion. In addition, these concepts are applicable to pipes of varying sizes and are capable of being developed into a remote diagnostic procedure for crevice corrosion. Such a procedure is adaptable to portable instrumentation for the detection of crevice corrosion within an assembled gasketed pipe joint. This instrumentation which will eliminate the requirement for disassembly and visual inspection of pipe joints and will be of great benefit to the Navy.

3.0 BACKGROUND ON CREVICE CORROSION

3.1 Mechanisms of Crevice Corrosion

Crevice corrosion is a localized form of corrosion which is inherent to metals and alloys that are easily passivated, such as Alloy 625. These include stainless steels, aluminum alloys, titanium, titanium alloys, and nickel based alloys. Although these materials normally exhibit excellent corrosion resistance due to their inherent ability to form a passive film, they are susceptible to corrosion at areas which are shielded by gaskets, washers, bolt heads, o-rings, barnacles, or other surface deposits. Iron and mild steels are also susceptible to crevice corrosion in highly oxidizing environments. Copper based alloys also exhibit crevice corrosion with the attack generally occurring just outside of the crevice itself [Moran, 1986; Laque, 1975].

Crevice corrosion attack generally results from compositional differences of the electrolyte within the crevice relative to that in the bulk. There is one type of crevice corrosion, referred to as electrolytic crevice corrosion, which results from anodic polarization of the crevice by a galvanic couple, or by potentiostatic polarization, without the necessity of a difference in the crevice environment from the bulk [France, 1972; Bombara, 1969; Strocchi et al., 1967].

Since this proposal concerns crevice corrosion for passive alloys, the widely accepted four step process for the crevice corrosion of stainless steels in neutral pH environments containing chloride presented by Fontana and Greene [Fontana and Greene, 1967], and later detailed by Oldfield and Sutton [Oldfield and Sutton, 1978], is discussed below.

The first step involves depletion of oxygen and other oxidants in the crevice environment. In neutral pH environments, such as sea water, the predominant cathodic reaction is oxygen reduction. Initially the small passive anodic currents in the crevice region, the same magnitude as those outside the crevice region at this stage, are balanced by the oxygen reduction reaction inside the crevice. The availability of new dissolved oxygen for the reaction is limited by the crevice geometry and eventually (can be as short as hours for very tight crevices) the cathodic reaction balancing the crevice anodic reactions shifts to the external surfaces where oxygen is more plentiful. This causes a buildup of excess positive charge inside the crevice, from the metal cations which are slowly dissolving, and leads to the second step. In chlorinated sea water there are additional cathodic reactions due to the oxidants created by the chlorination process. However, these cathodic reactants, like the dissolved oxygen, will be depleted in the crevice by the same mechanism.

The second step involves the continued metal ion buildup in the crevice, due to the anodic reaction there, and the migration of chloride from the bulk environment into the crevice region driven by the charge difference between the crevice region and the outside which results from step one. The metal chloride complexes resulting from this migration

6

hydrolyze, forming H^+ ions and lowering the pH in the crevice environment. This drop in pH and the increase of the chloride concentration are undesirable for the maintenance of the passive film. The extent to which the acidity increases and the chloride concentration increases depends heavily on the crevice tightness. Tighter crevices restrict diffusion and mixing of the bulk environment with the crevice environment and lead to more aggressive crevice chemistries.

The third step involves the permanent loss of passivity of the metal or alloy inside the crevice. The mechanism by which this occurs varies depending on the metal or alloy. Two mechanisms, relevant to our phase I proposal, are described. Pertinent to both is the change in the potential of the crevice region caused by step one. The decrease in oxygen in the crevice region, step one above, causes the potential of the crevice region to shift to much lower values than the external region. From a galvanic corrosion viewpoint, one would expect that the lower potential of the small crevice area would easily be polarized back to the potential of the external surface because of the much larger area of the external surface. This, however, is not the case. The relatively large ohmic resistance of the narrow electrolyte path in the crevice prevents the two regions from coming to the same potential. There is a potential drop, or an IR, caused by this narrow electrolyte path. The two regions are shifted toward the potential of the other from what would exist in the absence of the other, but the extent of this shift is limited by the IR of the crevice electrolyte path. Numerous investigators have measured negative potentials, some as high as 2V, for the crevice region relative to the potential for the external surface for iron, steel, stainless steel, and titanium alloys [Rosenfield and Marashov, 1964; Pickering and Frankenthal, 1972; Greene et al., 1965; Turnbull and Gardner, 1981; Chen et al., 1971; Pickering and Frankenthal, 1974; Pickering, in press; Valdes and Pickering, in press; Valdes and Pickering, 1987]. During the initiation of crevice corrosion the potential of the external surface decreases due to the galvanic coupling of the active crevice and the external cathode. Using a remote crevice configuration, Kain and Lee [Kain and Lee, 1983] observed negative shifts of the open circuit potential of the external surface of 316 and 18Cr-2Mo stainless steel with onset of crevice corrosion in sea water. Kain and Klein also observed negative shifts of the open circuit potential of Alloy 625 during the onset of crevice corrosion in remote crevice tests in natural sea water [Kain and Klein, 1990].

One possible consequence of the development of the aggressive crevice environment is a decrease in the passive film breakdown potential for the metal or alloy involved. If the breakdown potential is lowered sufficiently and the crevice potential, balanced by the external potential and the ohmic resistance of the crevice electrolyte path, is maintained above this potential, then the crevice material corrodes actively by a "breakdown mechanism". This has been discussed in the literature for a variety of stainless steels [Wilde and Williams, 1971; Kroughman and Ijsseling, 1980; Kain and Lee, 1983; Dawson and Ferreira, 1986; Dayal et al., 1983; Uhlig and Reevie, 1985; Pickering, 1986; Shaw et al., 1988; Kain, 1982; Kain et al., 1984; Sedriks, 1979]. Another possible consequence of the development of the aggressive crevice environment is a change in the polarization characteristics of the crevice material prior to breakdown.

The general change in the polarization behavior of stainless steel and nickel based materials caused by increased chloride and decreased pH are illustrated in Figure 1 The changes which result from increased chloride concentration and decreased pH are; 1) decrease in the breakdown potential, E_{bd}, (discussed in the breakdown mechanism), 2) increase in the passive current density, i_p, 3) increase in the critical current density, i_{crit}, necessary for passivity to occur (or the current density value at the "nose" of the active-passive transition), and 4) increase in the passive potential, i_{pp}. If the crevice potential, again balanced by the cathodic reactions occurring on the external surfaces and the crevice electrolyte path resistance, corresponds to a high current density region of the polarization behavior, such as in the active-passive region, crevice corrosion will ensue. This mechanism has been referred to as "IR induced crevice corrosion" [Shaw et al., 1988] because the IR due to the crevice electrolyte path causes the potential of the crevice to remain in a high current density region of the polarization curve (but below the breakdown potential). Shaw and Moran have demonstrated that this IR induced crevice corrosion mechanism is the one responsible for crevice corrosion of Alloy 625 in sea water [Shaw et al., 1991].

The fourth step in the crevice corrosion process is the propagation stage where the now actively corroding crevice is driven by the cathodic reactions occurring on the external surfaces. Biofilms, if present on the external surfaces, promote additional cathodic reactions and can thereby promote additional crevice corrosion as well as general corrosion. In a recent article and a related discussion article Dexter discusses the positive shift in corrosion potential and the increase in corrosion caused by biofilms for stainless steel and nickel based materials [Dexter and Gao, 1988; Dexter, 1989]. Enhancement of the cathodic reactions by the biofilm is generally accepted as the reason for accelerated corrosion by biofilms. Chlorination produces oxidants which destroy or inhibit the biological growth but which also supply additional cathodic reactions to the external surfaces. If the oxidant concentration produced by the chlorination was at exactly the right concentration to inhibit the biological activity, i.e. exactly meets the biodemand, corrosion processes would be expected to actually decrease. If, however, the chlorination exceeded the biodemand the additional cathodic reactions caused by the excess oxidants could promote additional corrosion.

An extremely important aspect of propagation relevant to this proposal is that a measurable ionic current flows in the solution. This current emanates at the site of crevice corrosion and flows out of the crevice to the external surfaces which support the cathode reaction and which control the rate of propagation. The development and demonstration of several methods for the proper detection of this ionic current constitute the primary focus of this proposal.

In summary, crevice corrosion initiation depends on whether the specific combination of alloy composition, crevice geometry, and bulk environment chemistry can provide a sufficiently aggressive crevice environment to interfere with the passivity of the alloy in the crevice. The extent of ensuing propagation, assuming initiation, depends on

the aggressiveness of the crevice solution chemistry (pH and chloride concentration), the external cathodic processes, and on the IR drop inside the crevice

3.2 Crevice Geometry and Crevice Corrosion

For a metal or alloy susceptible to crevice corrosion, the initiation is generally faster and the attack generally worse for a tighter crevice. A tighter crevice has less solution and therefore less dissolved oxygen than a looser one. Consequently, the time to deplete the dissolved oxygen is faster and the concentration of chloride and metal ions build-up faster. This leads to faster initiation times. The aggressiveness of the crevice solution increases with the tightness of the crevice as diffusion and mixing with the external environment are less likely with a tighter crevice. Brigham [1981] demonstrated for a 3.9% Mo stainless steel that crevices formed by elastic crevice formers, such as a rubber band, were more likely to initiate crevice corrosion in a 10% ferric chloride aqueous solution than looser crevices formed by materials such as glass, wood, and plastics which flow like nylon and polytetrafluoroehtylene (PTFE). The temperature at which any given percentage of the sites exposed initiated for the elastic material crevices was at least 15 ^{o}C lower than that for the same initiation percentage with the non-elastic crevice formers. He further demonstrated that surface finish had a profound influence on crevice corrosion. The likelihood of initiation increased for a roughened surface relative to a smoother surface (for the same crevice former). This observation was rationalized due to the tighter crevices formed by the peaks in the roughened surface.

The influence of the particular crevice-former on both the initiation and propagation stages of crevice corrosion, and therefore on the severity of attack, is important in comparing crevice corrosion behavior from one test to another. Comparisons of different product forms or of different environmental conditions can only be done for crevice formers which produce approximately the same tightness.

4.0 TECHNIQUES FOR REMOTE DETECTION OF CREVICE CORROSION

4.1: DC Measurement of Crevice Corrosion Current

As discussed above actively corroding crevices of most passive alloys, including Alloy 625, are coupled galvanically to the exposed surfaces outside the crevice. Consequently, an electrochemical current, essentially a galvanic corrosion current, flows between the crevice site and the external surface. This current can be detected.

4.2: AC Measurement of Crevice Corrosion Current

The structure which contains the crevice site can be driven with a low frequency (approx 1 to 10 Hz) low amplitude (approx 20 mV) voltage signal with respect to a remote electrode incorporated in the probe. This will cause a current of the same frequency to flow from sites of low impedance (low resistance). Since crevice corrosion sites have a low surface impedance because the passive film has been destroyed or damaged, the AC current will emanate preferentially from the crevice sites. A low frequency must be used to insure that the dielectric properties of the passive film on the material outside of the crevice continue to function as an insulator (or a relatively high impedance). The AC current which preferentially enters the solution at the crevice sites can be detected with the two electrode probe if the voltage signal between the two electrodes of a two-electrode probe is monitored with a lock-in amplifier operating at the same frequency as that applied to the structure. The two electrode probe can then be scanned along the surface of the structure to determine the crevice corrosion sites Lillard, Moran, and Issacs [1992] have recently demonstrated the feasibility of measuring AC currents in solution by this technique and have generated full AC impedance information over a broad range of AC frequencies for selected sites. Extremely small currents were successfully measured in their study.

4.3: Magnetic Field Measurement of Crevice Corrosion Current

This technique is an extension of Method 2 described above. The application of the AC signal in Method 2 will result in an AC current flow in the electrolyte. This current flow will occur predominantly at the crevice sites. An AC current in the electrolyte (or in any media for that matter) results in the generation of a magnetic field whose field strength is proportional to the magnitude of the current. By measuring the AC magnetic field at the same frequency as the potential perturbation frequency, the crevice corrosion sites can be detected. Murphy, Moran, et al have utilized this approach to successfully detect corrosion sites on buried pipelines [Murphy et al., 1988; U.S. Patent 5,087,873]. The magnetic field which results from current leaving a crevice site is complicated because, while the current leaves in predominantly a perpendicular manner, it turns away in all directions in a complicated fashion as it returns to the external surfaces. However, the magnetic field is relatively well characterized and strongest at the site of the crevice corrosion. Here a magnetic field emanates away from the perpendicular current. A small magnetometer aligned intentionally to measure this magnetic field will be scanned along the surface of the structure (in the electrolyte) and the sites of maximum magnetic field detected.

5.0 EXPERIMENTAL SETUP

5.1 Instrumentation and Apparatus

Figure 2 shows the instrumentation diagram along with the apparatus used for the studies. Magnetometer is a rectangular box of dimensions 3.5cm x 3.5 cm x 15.3 cm from

ElectroMechanical Design Services(EMDS). The sensing coils are 1in x 1in placed at the front end of the magnetometer. We used a Keithly 197A model 5-1/2 digit Voltmeter to read the output from the magnetometer for DC current fields. For AC measurements, we used EG&G 5210 lock-in-amplifier for the magnetometer's signal processing. We used a HP signal generator for sinusoidal potential waveforms which also used as reference signal for the Lock-in-Amplifier. An EG&G PAR 273 served as a galvanostat for both DC and AC measurements. For AC measurements, the waveform generated by the HP Function synthesizer is galvanostatically maintained by the PAR 273 and connected to the sample through EG&G electrochemical interface. The contacts to the plate are covered with an epoxy. The return electrode is a 1 in x 1 in platinum screen.

We conducted cell ecperiments in a plexi-glass trough of 2ft. x 3 ft. x 3 in. which was half-filled with 3.5 wt.% NaCl solution. Aeration is done to enhance the crevice corrosion. Inorder to ensure repeatability of the magnetic field measurements, we constructed a stage with leveling screws. The upper plate is manually leveled. The track for magnetometer is aided by a guide placed on top plate. The magnetometer is moved from place to place for magnetic field measurements. The specimen is kept underneath the stage exactly aligned with the magnetometer track. The position of the return electrode was varied in order to enhance magnetic detection of the crevice site.

5.2 Magnetic field components

The directionality of magnetic flux lines induced by a current lines in one direction can be best described by the right hand thumb rule. The right hand thumb rule involves grasping the current element in the right hand with the extended thumb pointing in the direction of the current. The fingers then encircle the element in the direction of flux lines. The magnetometer measures the flux density which is number of magnetic flux lines per unit area or the filed strength in gauss.

The relation between magnitude of dB, magnetic field flux density at point P, to the current element of length dl and current, i, is given by the Ampere's law (Fig. 3):

$$dB = k' \, i \, dl \, \sin\theta / r^2$$

where r is the distance between dl and the point P, and θ is the angle between r and dl. and $k' = \mu_0/4\pi$ according to Biot-Savart's law (Sears and Zemansky, 1950). Here, μ_0 is permittivity of the medium.

At a given distance r from the element the flux density is a maximum in a plane passing through the element perpendicular to its axis, since $\theta = 90^\circ$ and $\sin\theta = 1$ at all points.

In our case, since a thin strip of metal plate aligned with the magnetometer y-component direction, the magnetic field due to the current flowing in the strip would give

11

rise to the maximum flux densities in z and x components. Since the current lines are always aligned with y-z plane of the magnetometer, the maximum flux densities occur in the x-z or y-z planes depending on the current flow direction. The following table lists the important relationships between the current flow directions and resulting magnetic flux densities for our experimental conditions.

$$x \uparrow$$

$$y \longleftarrow \otimes z$$
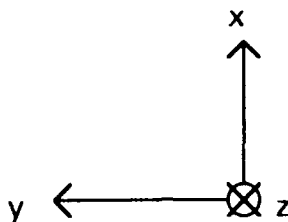
Current Flows	Magnetic Component
I_y	B_z, B_x
I_z	B_y, B_x
I_x	B_y, B_z

The current flow directions listed in the above table refers to that respect to the magnetometer magnetic field components. Specifically I_y and I_z are the current flow directions that are encountered in the experimental setup described in Figure 2. The maximum values for the magnetic field densities occur in z-direction and y-direction respectively. x-component can result when the metal strip is not aligned perfectly with y-z plane of the magnetometer.

6.0 RESULTS AND DISCUSSION

6.1 Sensitivity Measurements

In this study, we determined the sensitivity of the magnetometer for its response to both electronic current in the metal sample and ionic current in the solution and combination of both electronic and ionic. In the real piping system, our interest lies in the determination of ionic currents near crevice corrosion sites. We simulated various situations with our experimental setups to mimic the situations that may occur with the real pipe measurements. In order to attain uniform current density for ionic current flow, we designed a rectangular tough with parallel platinum electrodes facing each other. Two platinum foils of thickness 0.025mm of equal size (1.0 in x1.0in) are glued to opposing sides of plexi-glass trough. The dimensions of the plexi-glass trough are 1 in x 1 in x 12 in.

(See Figure 4). The following sections describe the results obtained with DC and AC currents respectively.

6.1.1 DC Sensitivity Measurements

Figure 5 shows the Magnetometer sensitivity with ionic DC currents. The schematic shows the directions for the ionic currents with respect to the magnetometer's measured vector directions. We used a 5-1/2 digit Keithly 197A model voltmeter for magnetic measurements with the DM-ALN60 magentometer. 10 volts equals 1 gauss magnetic field reading. The most significant component of the magnetic field measurement is in z-direction as the ionic flow is parallel to y-direction of the magnetic field measurement and in the y-z plane. y-component should be zero as the the magnetic field generated due to the current elements in y direction is zero. X-component is also zero as the the currents are parallel with y-z plane of the magnetometer. Small x-component values for magnetic field indicate that the plate is not perfectly flat with the calibration cell. The plot shows a linear relationship between the applied current density with the magnetic field measured by the magnetometer. The area used for calculation of current density is 1 in x 1 in. We determined the noise in the measurements by watching the voltmeter over a day. The readings fluctuated up to 100 millivolts. It gives a noise measurement under DC conditions to around 10^{-3} gauss. The noise, i.e., 10^{-3} gauss, affected the DC sensitivity with ionic currents which seems to be around 2.0 mA/cm^2. See Figure 5.

For combination of ionic flow and the electronic current flow, we placed a c-304 plate underneath the calibration cell and electronic flow is kept in parallel direction as the ionic flow. Figure 6 shows the magnetic field measurements with for co-current (ionic vs. electronic). The magnitude of the response is approximately double that shown in Figure 5 with ionic flow alone. The sensitivity is still limited by the noise.

Figure 7 and Figure 8 show DC sensitivity measurements with electronic and ionic flows are opposite in direction to each other. The data in Figure 8 represent the situation when the electronic current flow is on top of the ionic flow representing an outside the pipe type of measurement. The data in Figure 7 represent a situation where one measures magnetic field from inside pipe with ionic flow being closer than the electronic flow to the magnetometer. In both cases, since the opposing current fields produce opposing magnetic fields, the measured magnetic field values are smaller compared to that shown in Figure 5 and Figure 6.

6.1.2 AC Sensitivity Measurements

The magnetometer is sensitive to the external noise from various sources such as mechanical, light and earth contractions. Most of these fluctuations occur at specified frequencies as the source of the noise. We measured various noise amplitudes at different frequencies. Figure 9 shows the measured values from locking in the signal from idle magnetometer. In these measurements, we isolated the magnetometer from known sources of current fields. The spectrum in Figure 9 shows a distinctive peaks at 12, 20 , 60 and

13

100. We characterized this noise as that from building vibrations, railroad noise, light and so on. The measurements with the frequencies less than 1 Hz is limited by the low limit on the lock-in-amplifier model 5210(EG&G). The actual noise at frequencies less than 1 Hz is reflected in our DC measurements.

The data in Figure 10 shows the magnetometer calibration measurements with the alternating ionic current fields. We picked 10 Hz frequency for our signal because of the low background observed for the magnetic fields as shown in Figure 9.
The data shows excellent linearity between the measured z-component magnetic field and the rms value of the current density. Figure 5.11 shows the expanded version of the Figure 10 for a maximum of current density 2 mA/cm^2. From the estimated noise level at 10 Hz, the sensitivity with alternating current fields is approximately 0.02 mA/cm^2. The typical current densities reported in the literature for crevice corrosion are as high as 100 μA/cm^2.

6.2 Remote Detection of Crevice Corrosion

We obtained 1in. x 17 in. x 1/8 in. c-304 stainless steel samples from Metal Samples, Inc Alabama. The as-obtained samples have a glass-bead finish (500 micron surface finish). We placed c-304 steel samples in aerated solution containing 3.5 wt.% NaCl reagent grade. As described in Section 5.1, we placed the magnetometer on top of a plexi-glass stage. We took the magnetometer readings along the plate starting from electrical contact to the plate.We covered the contact for the c-304 specimen with Duro master mend epoxy. The end position of the plate is 17 inches from the contact. The crevice sites were placed at the 9 inch position. A sinusoidal waveform of current with 10 Hz frequency and 35 mA rms value is used for all the subsequent experiments.

Our objective here is to determine the spatial resolution of the crevice sites with our magnetometer. In the initial experiments, we had difficulty in creating crevice corrosion on c-304 metal plates. Consequently, we used a steel bolt that was bolted in the plate at the 9 inch position. We selected a flat head of size 1/4 in. steel bolt that freely corrodes in the salt solution. The steel bolt in the plate represents a low impedance corrosion site compared to the passive film on c-304 plate. In the latter stages of our experiments, we attained actual crevice corrosion sites using o-rings on the plate to represent a gasketed junction. The details are described in Section 6.2.3.2.

In order to obtain maximum spatial resolution with magnetometer for detection of crevice sites, we tried three different positions for the return electrode as shown in Figure 12. The position 1 in Figure 12 refers to the position of the return electrode in the opposite side to the electrical contact of the plate. In this position, the ionic current in the solution flows in the same direction as the electronic current in the plate and hence 'co-current flows'. The position 2 refers to the position of the return electrode at the same side of the contact. Here the ionic current in the solution flows opposite to the electronic

current in the plate and referred as 'counter current flows'. The position 3 in Figure 12 refers to the position of the return electrode on the side of the plate close to the middle of the plate. In this situation, the ionic current flows perpendicular to the electronic current in the plate and referred as 'perpendicular current flows'.

6.2.1 Co-Current Flows

We placed the return electrode at 6 inches from the end of the plate. This end is opposite to the electrical contact or as position 1 in Figure 12. We placed a steel bolt in the plate around 9 inches. Figures 13 and 14 show the magnetic field measurements with plate immersed in the solution. The resulting ionic currents is on top of the electronic flow and closer to the magnetometer. The discoloration of the solution to yellow (Ferric Chloride) indicated rapid dissolution of the bolt. In both figures, we compared the data obtained from two plates; one with bolt and other one with no bolt. The 'no bolt' data represents data obtained for a plate with uniform surface without any visible corroding sites on the surface. Both plates are made of c-304 stainless steel. As expected with the y-direction current flows, the data shows significant values for z-component of magnetic field than others. The data shows no marked difference for the plate with a bolt in the plate.

Figures 15 and 16 show the data obtained with floating plates. The solution contact with plate is primarily on the bottom side of the plate, the resulting ionic flow of current is below the electronic current flow in the plate. In this case, the electronic flow is closer to the magnetometer. The plates are 1/4 in closer to magnetometer than the cases presented in Figures 13 and 14. The data show similar trends as the ones above. It showed significant z-component magnetic field measurement and failed to resolve the bolt in the plate.

We rationalized these data using the schematic shown in Figure 15. In the case of the plate with no site, the electronic current in plate drops uniformly and similarly, the ionic flow in the solution picksup uniformly. Since the ionic current and electronic currents are parallel, the net resulting current is constant and equal to the input current. In the case of a plate with site, the electronic current flow in the plate drops uniformly until the position of crevice site and then drops suddenly. Ionic flow in the solution complements the electronic flow to give a constant response. In this situation, one would not expect much sensitivity towards detecting crevice corrosion.

6.2.2 Counter Current Flows

We tried another position for the return electrode, i.e. on the same side as the electrical contact to the metal plate. The return electrode is approximately 9 inches away from the contact. The Figures 16 and 17 show the magnetic field measurements with the plates completely immersed in the solution. Even in this case, we compared the magnetic field measurements for two plates; one with a bolt and one without any corrosion sites. The data show lower magnitudes than that for Co-Current flows.

Figures 18 and 19 show the data obtained for the case that represents an outside the pipe measurement. The data show similar trend as Figures 16 and 17.

When we place the return electrode on the same side as the contact, the resulting ionic current flows in opposite direction to the electronic current flow in the plate. The net magnetic field will be sum of the two opposing fields created by the opposing current fields. See Figure 20. Theoretical values for net current is zero even with a corroding site on the plate's surface. The experimental measurements of the net magnetic field result from the difference in the current density and distance from magnetometer at each point. From the data obtained, we could not resolve the bolt in the plate with this return electrode position.

6.2.3 Perpendicular Current Flows

6.2.3.1 One Return Electrode

We placed the return electrode on the side of the plate and close to the middle of the plate as position 3 in Figure 12. The resulting ionic current flow perpendicular to the electronic current flow in the plate. The ionic flow is in the z-component direction of the magnetometer. The y-component of the magnetic field measurements represent magnetic field produced predominantly by the ionic currents leaving the plate in perpendicular fashion. The return electrode is approximately 2 inches away from the plate's edge. The Figures 21 and 22 show the data from the immersed plates. The comparison between the plate with no corrosion site show that y-component of the magnetic field from the corroding site at 9 inches gave a higher signal than that from the plate with a corrosion site. The net difference of these two magnetic fields indicates preferential leakage from the corrosion site.

Figures 23 and 24 show the data obtained when the plates are just above the solution only exposing the bottom side of the plate. The difference in the magnitudes of the magnetic fields is enhanced. These data show that much better sensitivity can be expected ith outside the pipe measurements.

The leakage from the plate with no site shows non-uniform leaking of current with maximum near the return electrode position in both cases, i.e., in the case of immersed plates and also in the case of floating plates. However, for a simpler implementation of this technique, we would desire a flat response with the plate with no site. In order to obtain the flat response with specimen leaking uniformly, we placed five return electrodes spaced equally from the plate.

6.2.3.2 Five Return Electrodes

We used o-rings on the c-304 plate in this experiment to create actual crevice corrosion sites. In the previous experiments, we mimicked the low impedance site with a steel bolt. In order to initiate crevice corrosion, we passed 20 mA of DC current through the

16

specimen for approximately 12 hours. We removed 20 mA DC current for subsequent experiments for determination of spatial resolution of the crevice sites with five return electrodes. Crevice corrosion was confirmed by subsequent visual inspection of the specimen.

We used five return electrodes to obtain uniform current distribution from the samples. The data in Figure 25 show only the y-component of the magnetic field. In this case, we used o-rings to create the crevice corrosion. The data shows flat y-component magnetic field as expected for uniform leakage from the plate with no o-rings on it. The plate with crevice corrosion sites show a maximum in y-component magnetic field at the site. The signal from the crevices is approximately double that from bulk surface of the c-304 steel. The enhanced component of the y-component magnetic field near the crevice site indicates that the current leaked preferentially from the crevice sites. The signal enhancement is also occured beyond the position of real crevice sites indicating low impedance surface sites along the plate's edges. The subsequent visual inspection of the plate revealed pits on the plate's edge beyond the position of real crevice sites.

6.3 Equivalent Analog Circuit Model Calculations

We rationalize our experimental observations with perpendicular current flows using equivalent circuit models. Figure 26 shows a discrete model of circuit used to model the c-304 plate. Each circuit element models a 1.0 length along plate surface. We assumed that the passive film acts as a capacitor in parallel with a passive film polarization resistor. In the case of a crevice corrosion site or active metal surface, the capacitor is the double layer capacitance in parallel with the faradaic resistance. Values for passive film capacitor and resistor are 120 micro-farads/cm^2 and 1250 ohm-cm^2 respectively. Corresponding values for the crevice corrosion site are 20 micro-farads/cm^2 and 1.25 ohm-cm^2 repectively. The area from 1.0 in. length of the plate is used for the calculation of the discrete values for the capacitors and resistors.

6.3.1 Effect of Solution Resistance

When we place only one electrode at a 5 in. from the plate(near crevice corrosion site), the resistances of the solution path from other circuit elements scale as the respective distances. Figure 27 shows the model calculations for the leakage current through each circuit element with a solution resistance of 110 ohm-cm. The leakage currents show a maximum at the place closest to the return electrode. In the case of crevice corrosion site, the leakage current close to double that from a non corroding site.

Figure 28 shows the calculations with a solution resistance value of 11 ohm-cm which is 10 times less that used for calculations shown in Figure 27. The calculations show that uniform leakage irrespective of the distance of the circuit element and the signal from the crevice corrosion site is enhanced. Figure 2 sh- v the calculations with increased solution resistance of 1100 ohm-cm. The data clearly shows that no distinction can be made between crevice corrosion sites and passive film when the solution resistance is

17

relatively high. This indicates that the increased solution resistance automatically affects the ability to detect the crevice corrosion.

6.3.2 Five Return Electrodes

Instead of one return electrode, five return electrodes are placed at 5 in distance from the plate as shown in Figure 30. The solution resistors in this case are all equal as they are equally distance from the return electrodes. The data (Figure 31) shows uniform leakage from passive film as all the solution resistors are all equal. The maximum signal from the crevice corrosion site is still equal to that from on return electrode. The increased solution resistance washes out the signal from the corrosion site compared to the passive film. Increasing the conductivity enhances the signal as shown in Figure 32. With increased conductivity, the size of the return electrode and the distance from the plate are immaterial for remote detection of the crevice corrosion. In the case of low conductive solutions, the return electrode should be placed close to that from the plate for the remote detection of crevice corrosion.

7.0 REFERENCES

Bombara, G.(1969), Corr. Sci., Vol. 9, p. 519.
Brigham, R.J.(1981), Corrosion, Vol. 37, No. 10, pp. 608-609.
Chen, C.M., Beck, F.H., and Fontana, M.G.(1971), Corrosion, Vol. 27, p. 234.
Crowe, C.R. and Kasper, R.G.(1986), J. Electrochem. Soc., Vol. 133 p. 879 (1986).
Dayal, R.K., Parvathavarthini, N., and Gnanamoorthy, J.B.(1983), Br. Corr. J.,
        Vol. 18, p.184.
Dawson, J.L, and Ferreira, M.G.S.(1986), Corr. Sci., Vol. 26, p. 1027.
Dexter, S.C., and Gao, G.Y.(1988), Corrosion, Vol. 44, No. 10, p. 717.
Dexter, S.C.(1989), Reply to Discussion of Ref. 37, Corrosion, Vol. 45, No. 10, p. 786.
France Jr., W.D., and Greene, N.D., Jr.(1968), Corrosion, Vol. 24, p. 247.
 France W.D(1972), Localized Corrosion - Cause of Metal Failure, ASTM-STP 516,
        p. 164, ASTM, Phila., PA.
Localized Corrosion, eds. R.W. Staehle, B.F. Brown, J. Kruger, A. Agarwal, National
        Assoc. of Corrosion Engineers, p. 623. 1974.
Strocchi, P.M., Sinigaglia, D., and Vincentini, D.(1967), Elec. Met., Vol. 2, p. 38.
Fontana M.G., and Greene, N.D.(1967), Corrosion Engineering, p.41,
        McGraw-Hill, New York.
Greene, N.D., France, Jr., W.D., and Wilde, B.E.(1965), Corrosion, Vol. 21, p. 275.
Isaacs, H.S.(1988), J. Electrochem. Soc., Vol. 135 p. 2180.
Isaacs, H.S.(1987), Corrosion, Vol. 43 p. 594.
Isaacs, H.S.(1988), Corrosion Science, Vol. 28, p. 547.
Jaffe, L.F., and Nuticelli, R.(1974), J. Cell Biology, Vol. 63, p. 614.
Kain, R.M., and Lee, T.S.(1983), Laboratory Tests and Standards, ASTM-STP 866,
        Amer. Soc. for Testing and Matls., Phila., PA, p. 299.

Kain, R.M., and Lee, T.S.(1983), Laboratory Tests and Standards, ASTM-STP 866,
Amer. Soc. for Testing and Matls., Phila., PA, p. 299.

Kain, R.M., and Klein, P.A.(1990), Corrosion '90 Paper No. 158, National Assoc. of
Corr. Engrs., Houston, TX.

Kain, R.M.(1982), Corrosion '82 Paper No. 66, National Assoc. of Corr. Engr.,
Houston, TX.

Kain, R.M., Tuthill, A., and Topsie, E.(1984), J. Materials for Energy, Vol. 5, p. 205.

Kain, R.M.(1984), Metals Handbook Vol. 13, ASM International, Metals Park, OH, p111.

Krougman, J.M., and Ijsseling, F.P.(1980), Proc. of the 5th Internat. Congress on Marine
Corr. and Fouling, Barcelona, Spain, p. 214.

F.L. LaQue (1975), Marine Corrosion Causes and Prevention, J. Wiley and Sons, p. 175.

Lillard, R.S., Moran, P.J., Isaacs, H.S.(1992), J. Electrochem. Soc., Vol. 139, No. 4,
p. 1007.

P.J. Moran (1992), U.S. Naval Academy, Private Communication.

Murphy, J.C., Hartong, G., Cohn, R.F., Moran, P.J., Bundy, K., Scully, J.R.(1988),
J. Electrochem. Soc., Vol. 135, No. 2, p.310.

Oldfield, J.W. and Sutton, W.H.(1978), "Crevice Corrosion of Stainless Steels",
British Corrosion Journal, Vol. 13.

Pickering, H.W., and Frankenthal, R.P.(1972), J. Electrochem. Soc.,
Vol. 119, p. 1297.

Pickering, H.W., and Frankenthal, R.P.(1974), Localized Corrosion, eds. R.W. Staehle,
B.F. Brown, J. Kruger, A. Agarwal, National Assoc. of Corrosion Engineers,
p. 261.

Pickering, H.W., Proc. Inter. Conf. on Localized Corrosion, ed. H. Isaacs,
National Assoc. of Corr. Engrs, Houston, TX (in press).

Rosenfeld, I.L., and Marashov, I.K.(1964), Corrosion, Vol. 20, p. 115.

Sears, F.W., and Zemansky, M.W.(1950), "University Physics", Addison Wesley Press,
Cambridge, Massachusetts, U.S.A.

Sedriks, A.J.(1979), Corrosion of Stainless Steels, J. Wiley and Sons, New York, p. 57.

Shaw, B.A.(1988), Crevice Corrosion of a Ni-Cr-Mo-Fe Alloy in Natural and Chlorinated
Seawater, Ph.D. Dissertation, The Johns Hopkins University.

Shaw, B.A., Moran, P.J., and Gartland, P.O.(1991), Corrosion Science, Vol. 32, No. 7,
p. 707.

Shaw, B.A., Moran, P.J.,and Gartland, P.O.(1988), Corrosion '88 Research Symposium
Abstract, National Assoc. of Corr. Engrs., Houston, TX.

Turnbull, A., and Gardner, M.K., Br. Corr. J.(1968), Vol. 16, p. 140.

Uhlig, H.H., and Reevie, R.W.(1985), Corrosion and Corrosion Control, J. Wiley and
Sons, New York, p. 316.

U.S. Patent No. 5,087,873, Non-Invasive, High Resolution Detection of Electrical
Currents and Electrochemical Impedances at Spaced Localities Along a Pipeline,
Issued Feb. 1992.

Valdes, A., and Pickering, H.W., Proc. Inter. Conf. on Localized Corrosion, ed. H. Isaacs,
National Assoc. of Corr. Engrs, Houston, TX (in press).

Valdes, A., and Pickering, H.W.(1987), Environmental Degradation of
Engineering Materials III, ed. M.R. Louthan, Jr., p. 227,

The Pennsylvania State Univ.
Wilde, B.E., and Williams, E.(1971), Electrochim. Acta, Vol. 16, p.1972.

E

E_{bd} ↓ WITH INCREASING Cl⁻

I_p → WITH INCREASING Cl⁻ AND [H⁺]

E_{pp} ↑ WITH INCREASING [H⁺]

I_{crit} → WITH INCREASING Cl⁻ AND [H⁺]

LOG i
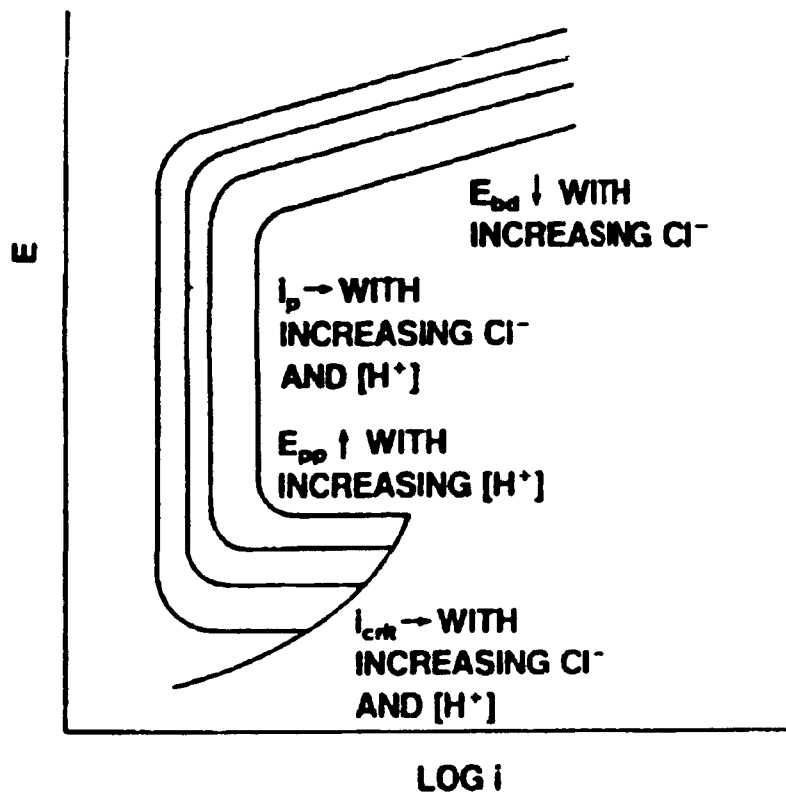
Figure 1: Schematic Representation of the Anodic Polarization Behavior in Increasingly Aggressive Environment within the Crevice (after Shaw, 1988).

Lock-in-Amplifier

Function Generator

1 Y Voltmeter
Keithly 197A

Magnetometer
console

PAR 273

sensing coils

Platinum mesh

Rubber bands

c-304 plate
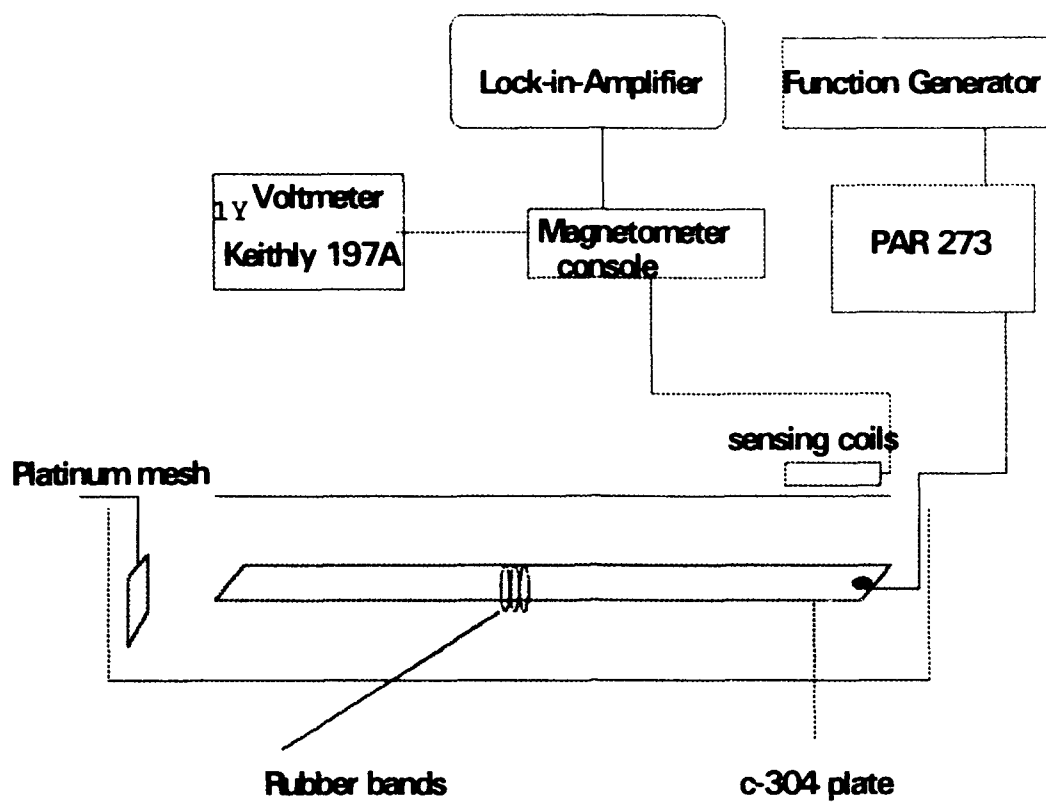
N01_B15

Figure 2: Experimental setup used for remote detection of crevice corrosion.

Instrumentation

Plexi-glass trough
filled with 3.5 wt.% NaCl

Magnetic Sensing Coils

Platinum

To Power
Supply

Metal Plate
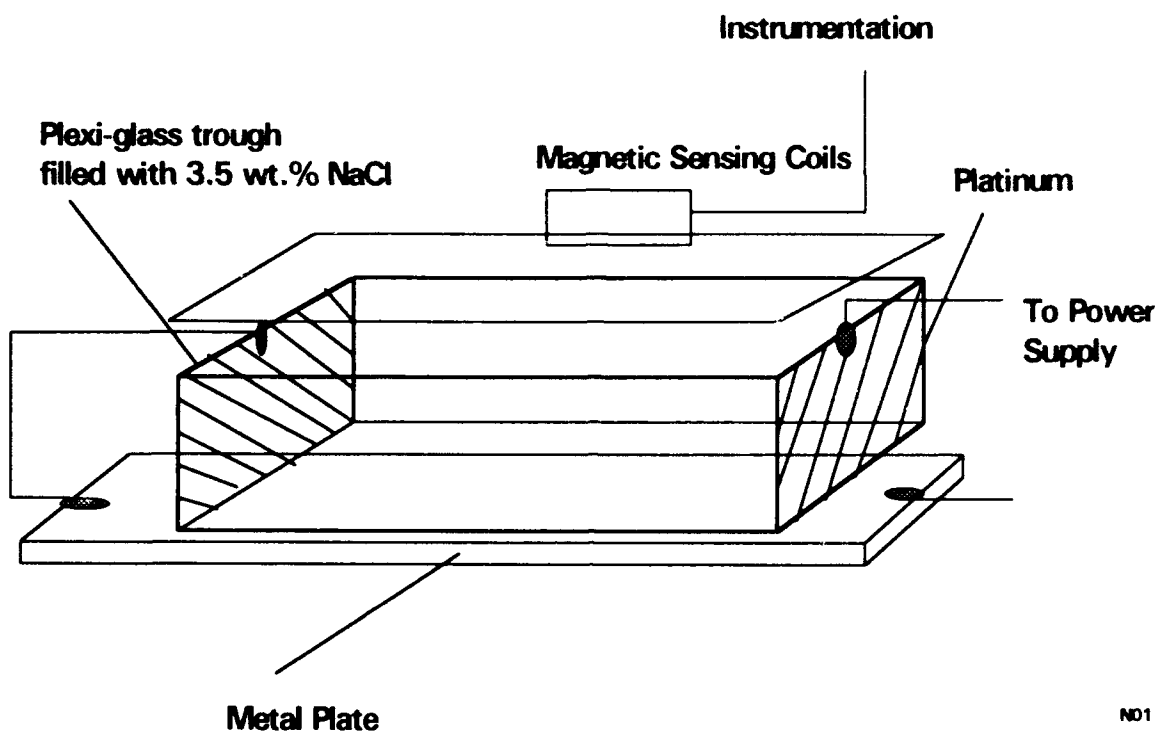
N01 807

Figure 3: Calibration cell setup used for sensitivtiy measurements
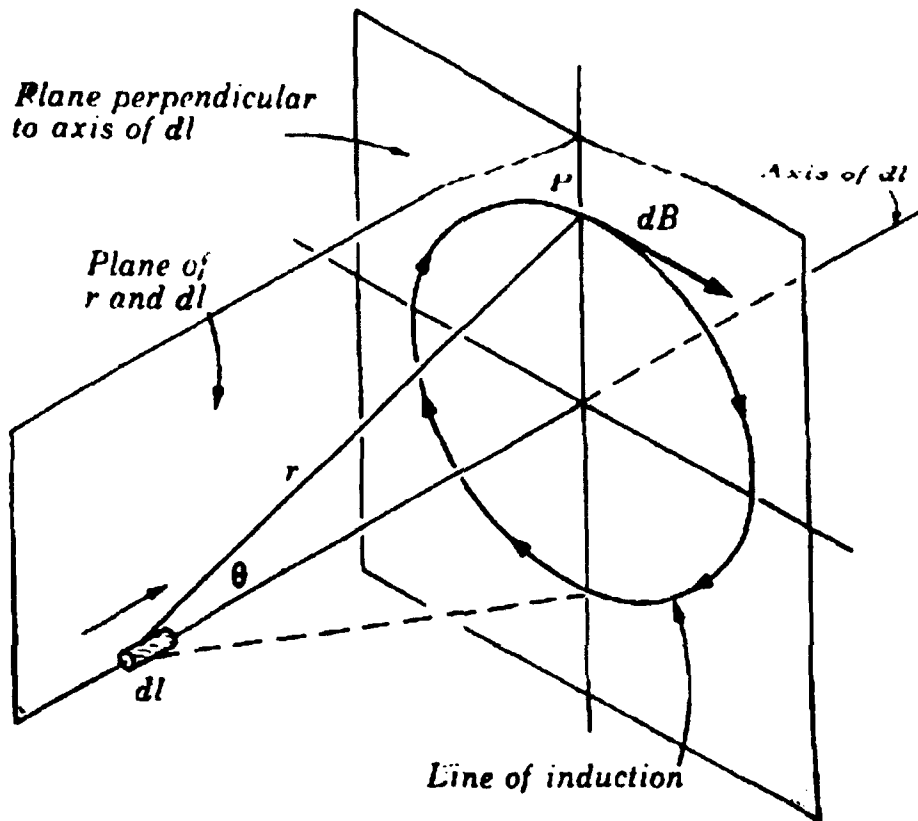
Figure 4: Magnetic field due to a current element (Sears and Zemansky, 1950)
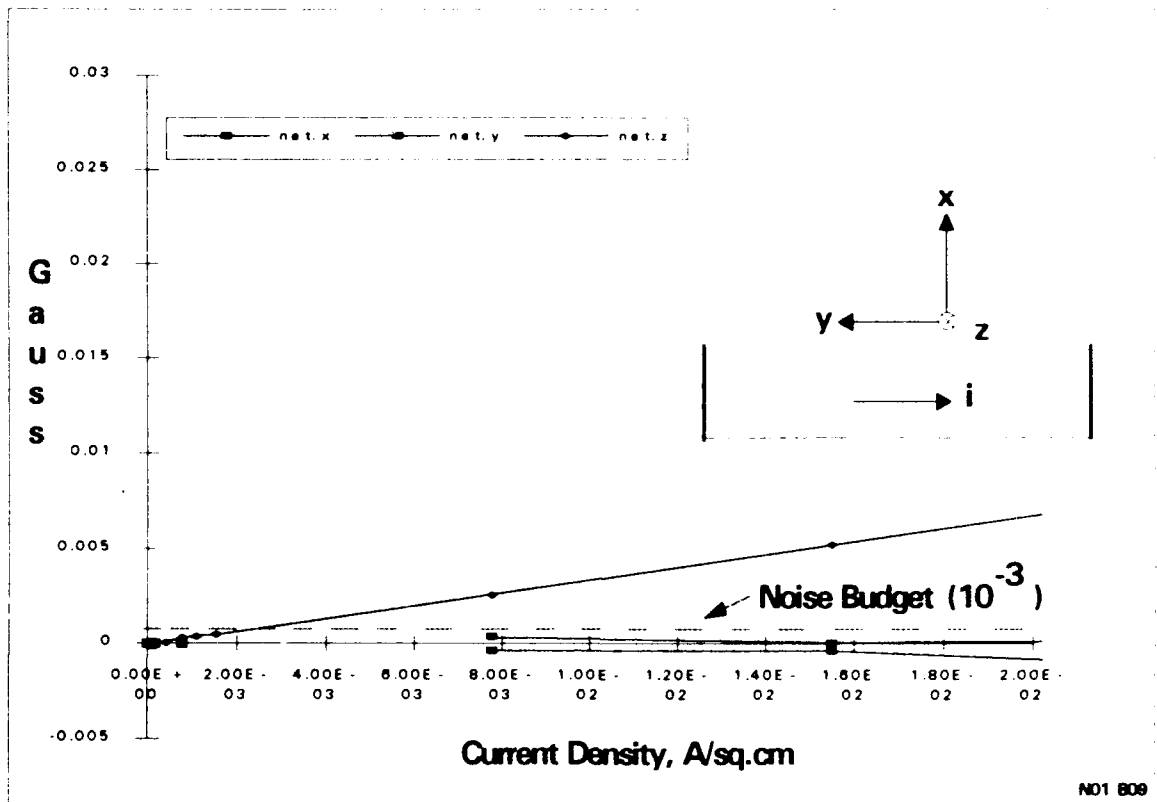
Figure 5.5: DC sensitivity measurements with the calibration cell with only ionic flow of current.
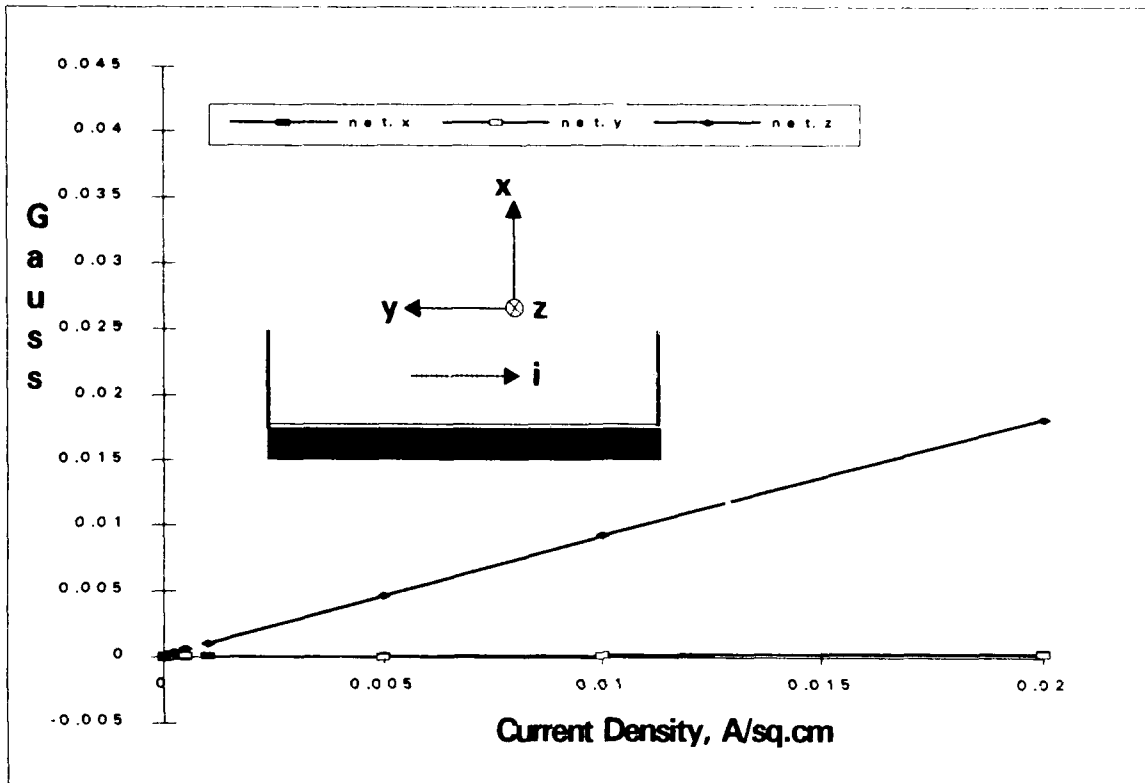
Figure 6: DC sensitivity measurements with electronic flow underneath the ionic flow but parallel in direction.
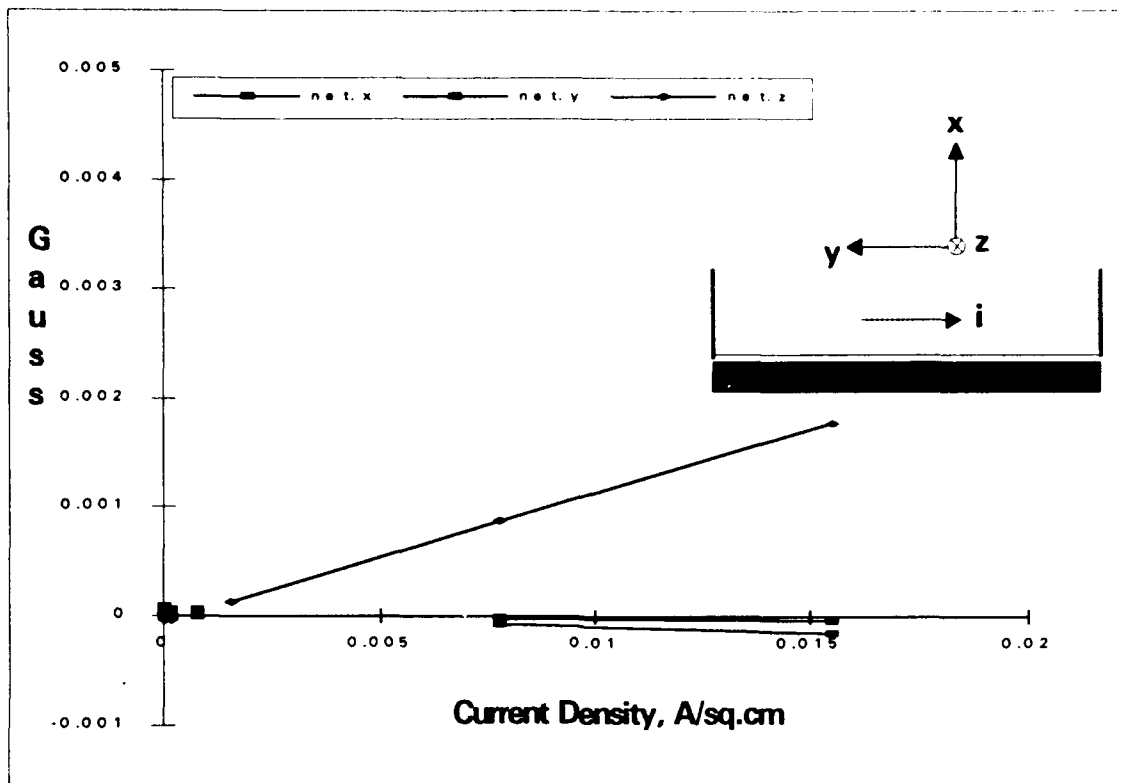
Figure 7: DC sensitivity measurements with electronic flow underneath ionic flow and opposite in direction.
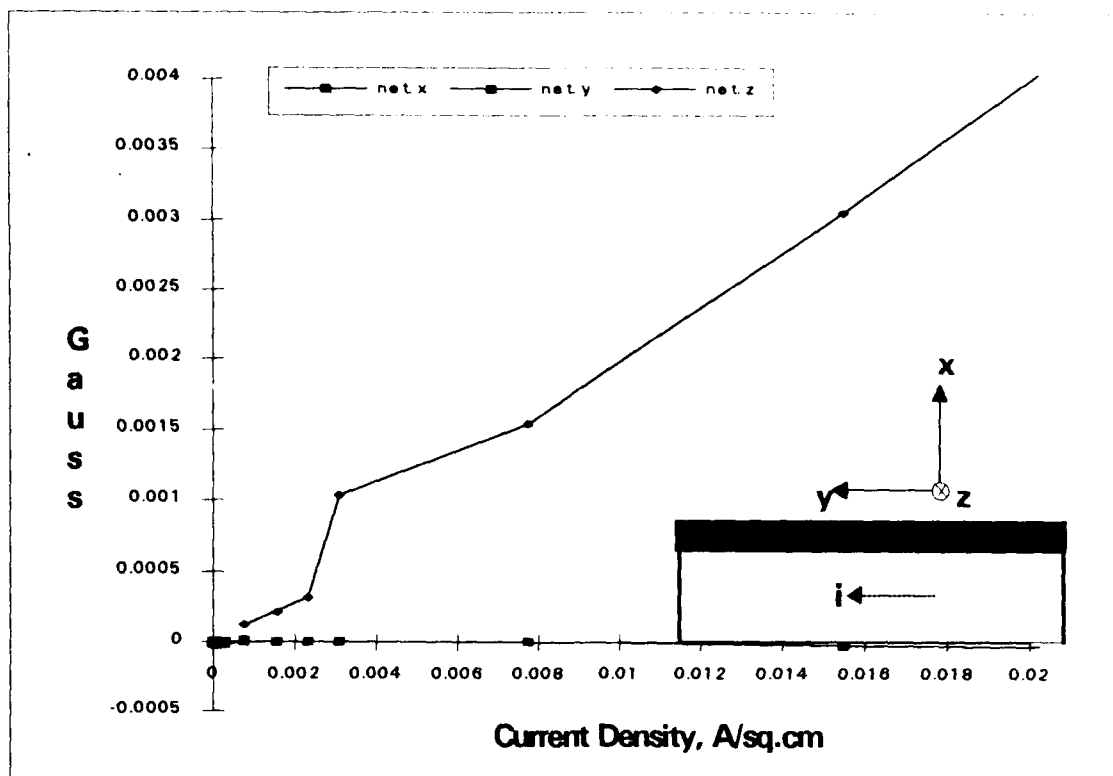
Figure 8: DC sensitivity measurements with electronic flow on top of ionic flow and opposite in direction.
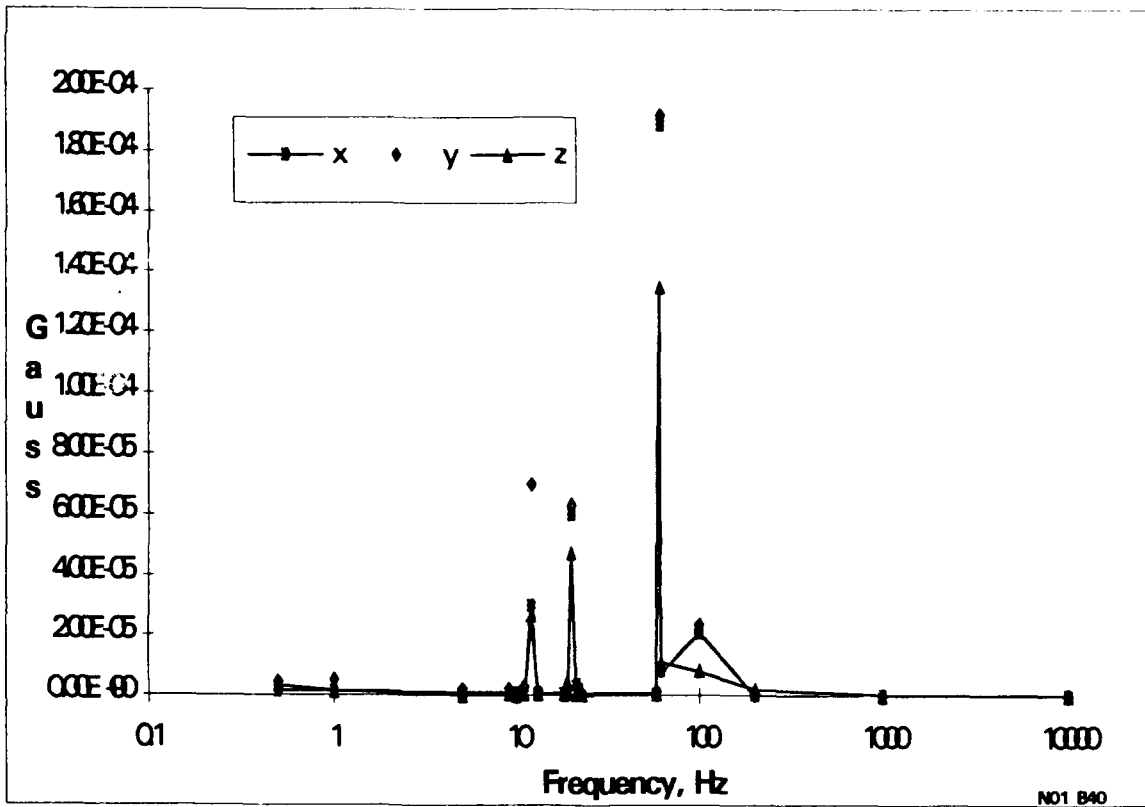
Figure 9: Background measurements with magnetometer at various frequencies.
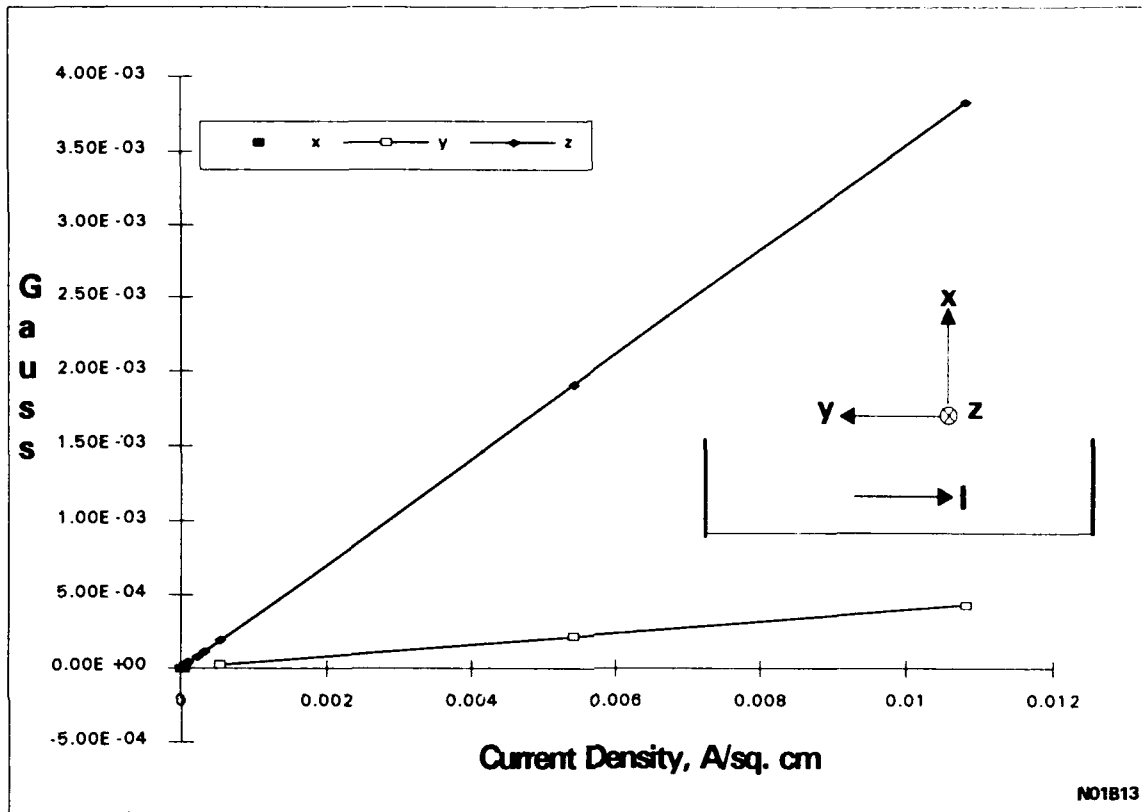
Figure 10: AC sensitivity measurements with magnetometer with 10 Hz signal and with ionic flow only.
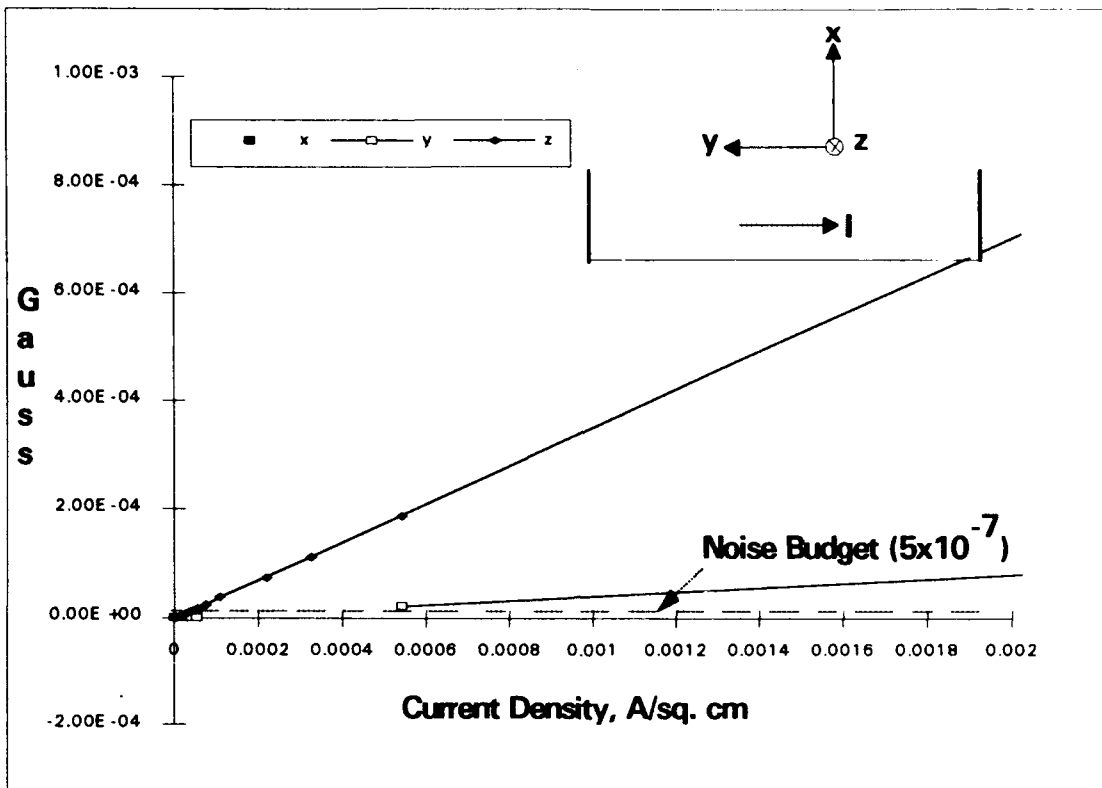
Figure 11: AC sensitivity measurements with ionic flow and 10 Hz signal. Expanded version of Figure 10.
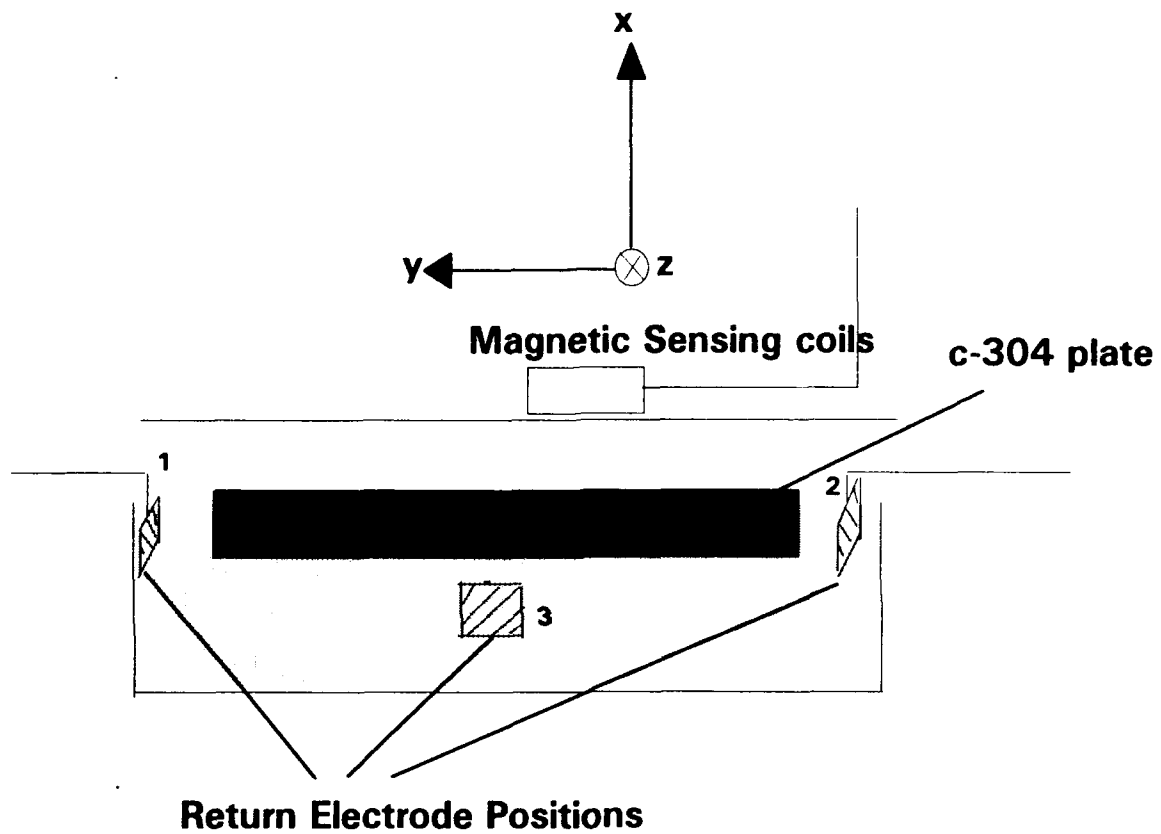
Figure 12: Schematic of experimental setup showing the three different positions used in this work for return electrode.
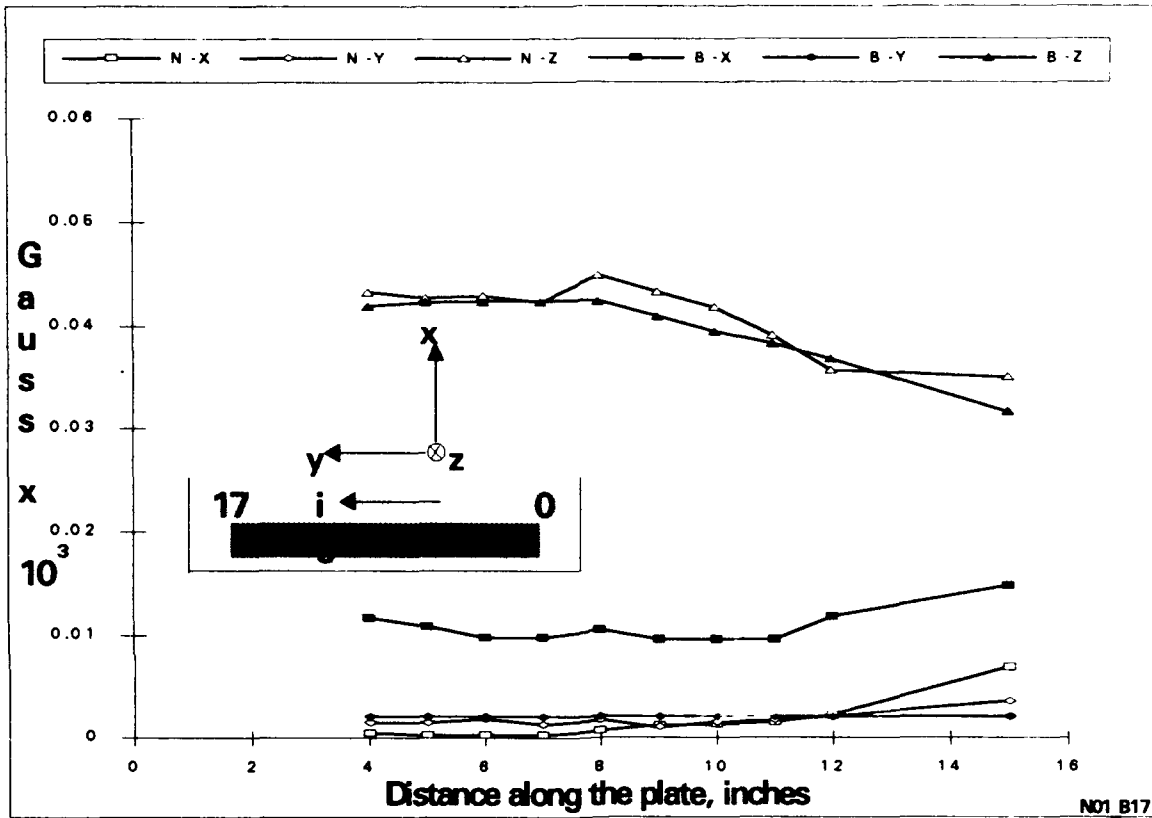
Figure 13: Co-current flows: Magnetic field measurements over a submerged strip with a steel bolt at 9 inches.
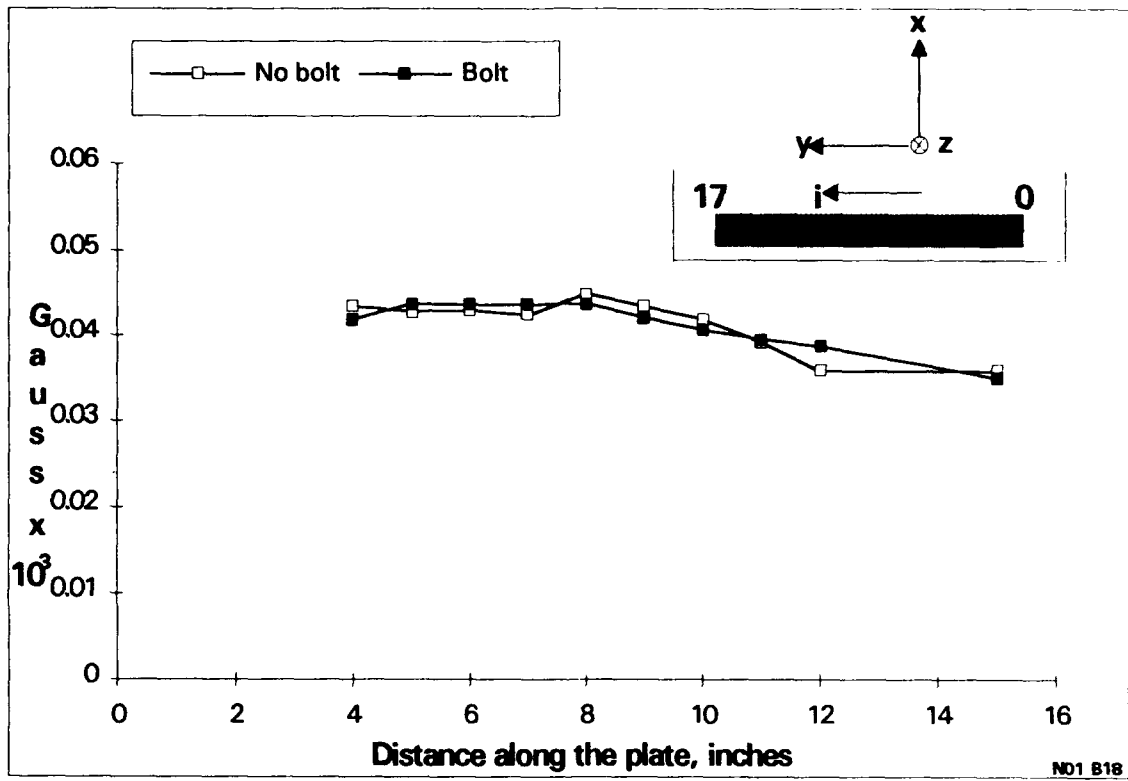
Figure 14: Co-current flows: rms values of magnetic field measurents shown in
Figure 13.
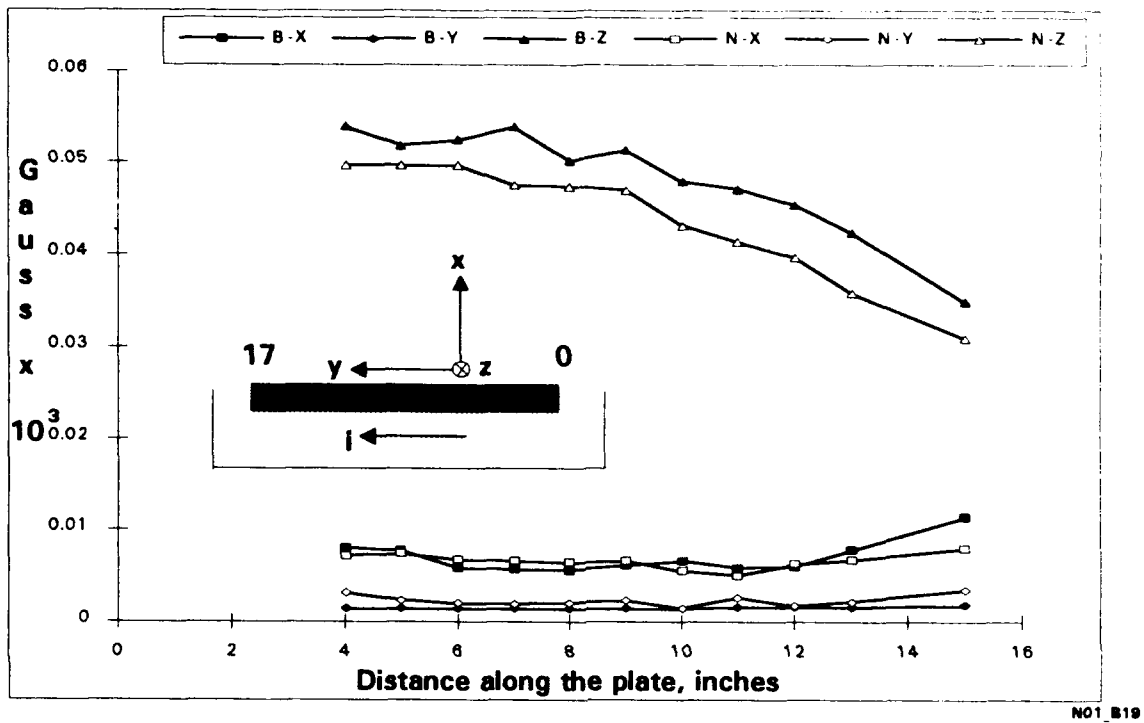
Figure 15: Co-current flows: Magnetic field measurements on floating c-304 plate with a
bolt at 9 inches.
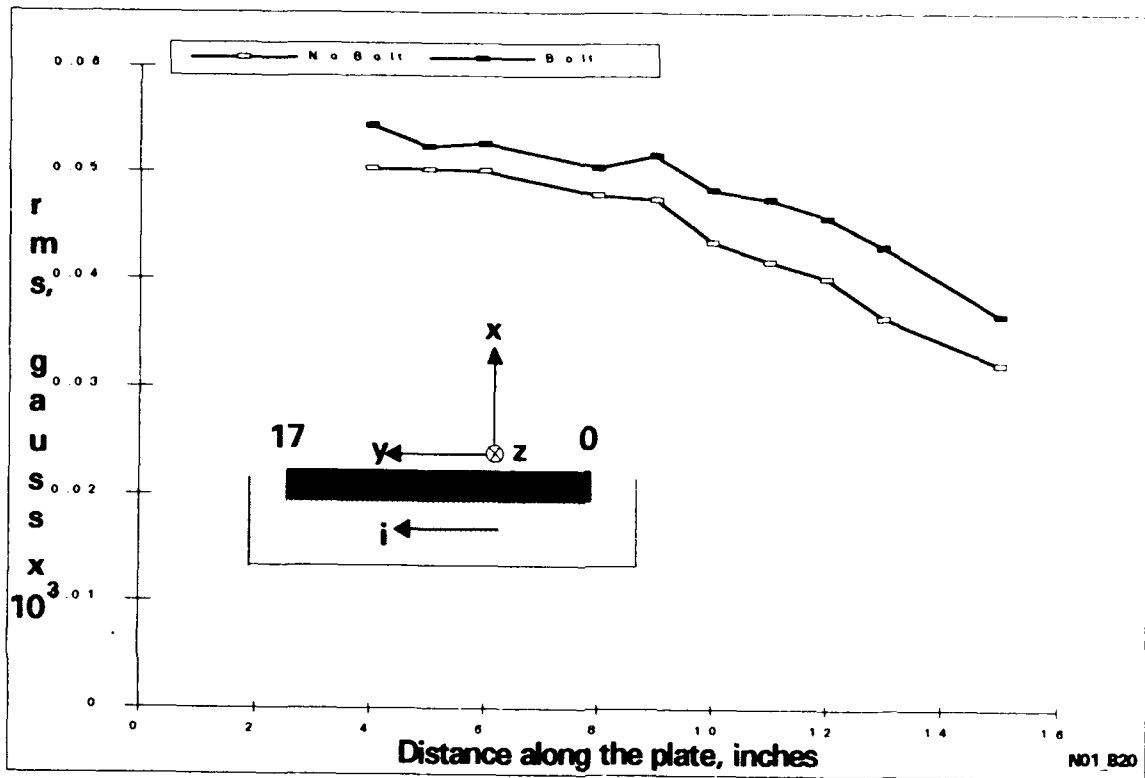
Figure 16: Co-current flows: rms values of the magnetic field measurements shown in
Figure 15.

No Site

total

ionic

electronic

I

Distance

Site

total

ionic

electronic

I
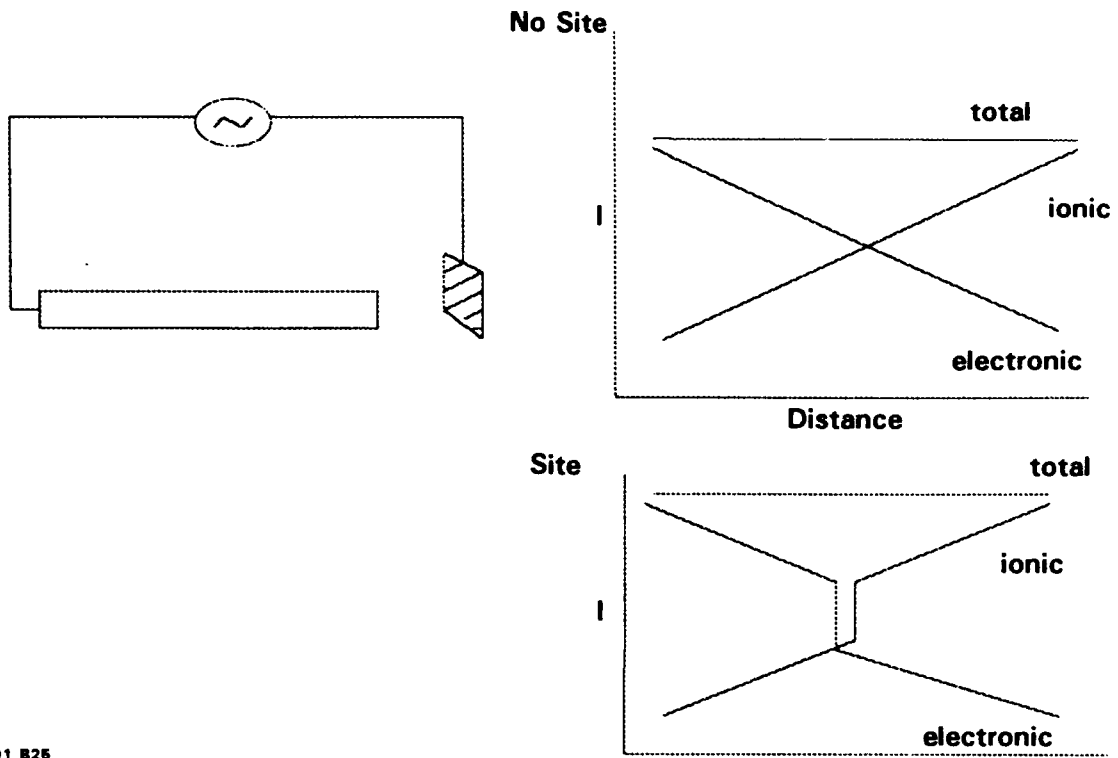
NO1_B25

Figure 17: Schematic of the situation with co-current flows showing the individual ionic, electronic and net total current components for subsequent magnetic field measurements.

37
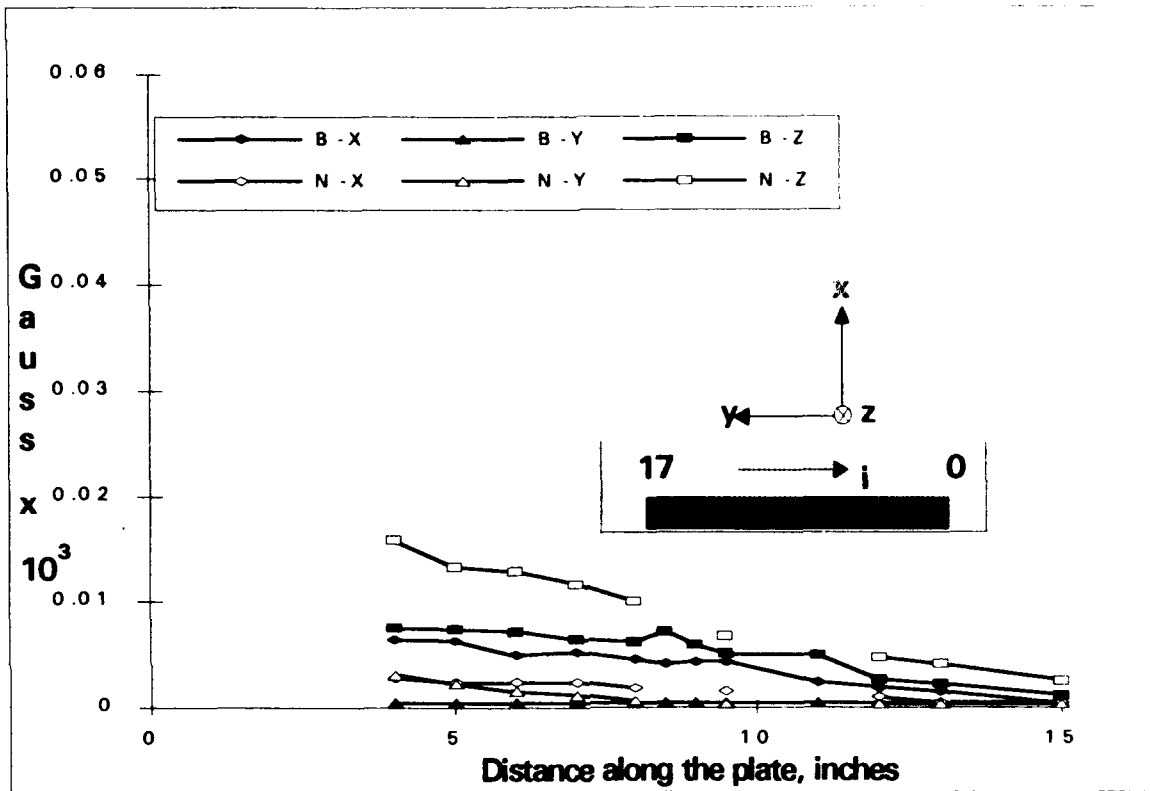
Figure 18: Counter-current flows: Magnetic field measurements on a c-304 metal strip with a bolt at 9 inches.
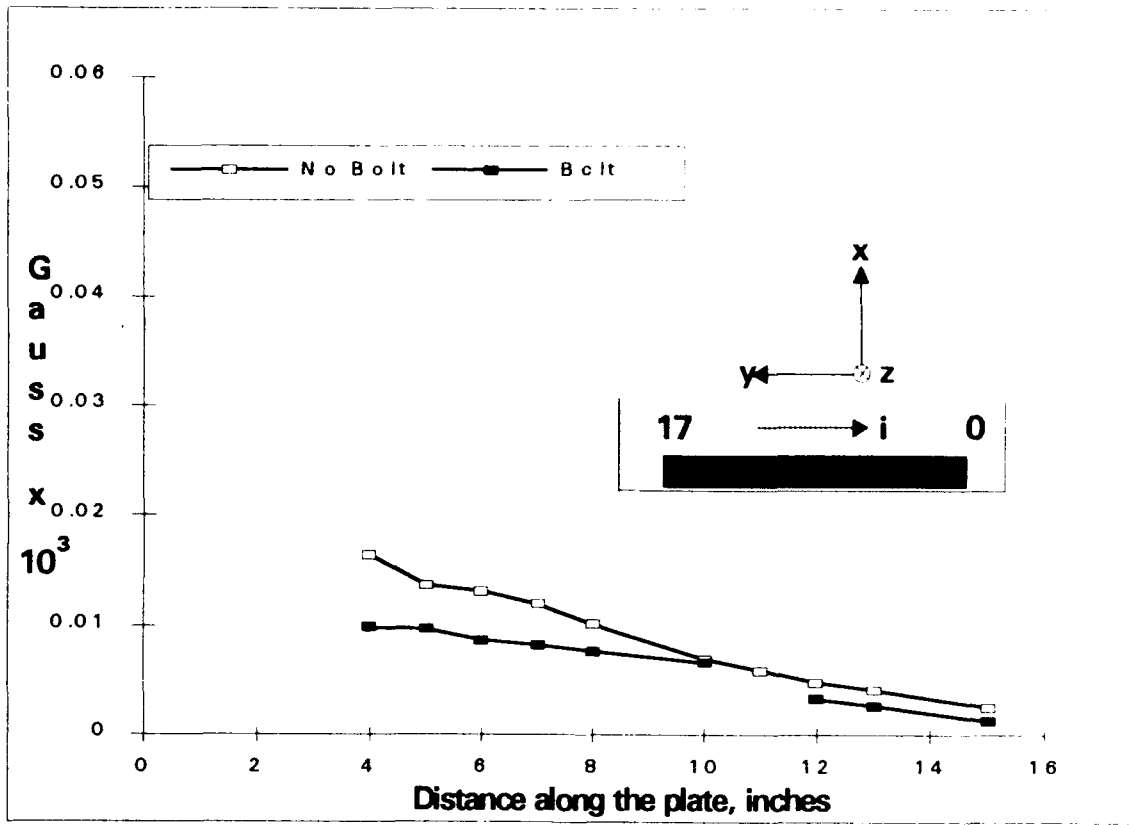
Figure 19: Counter-current flows: rms values of the magnetic field measurements shown in Figure 18.
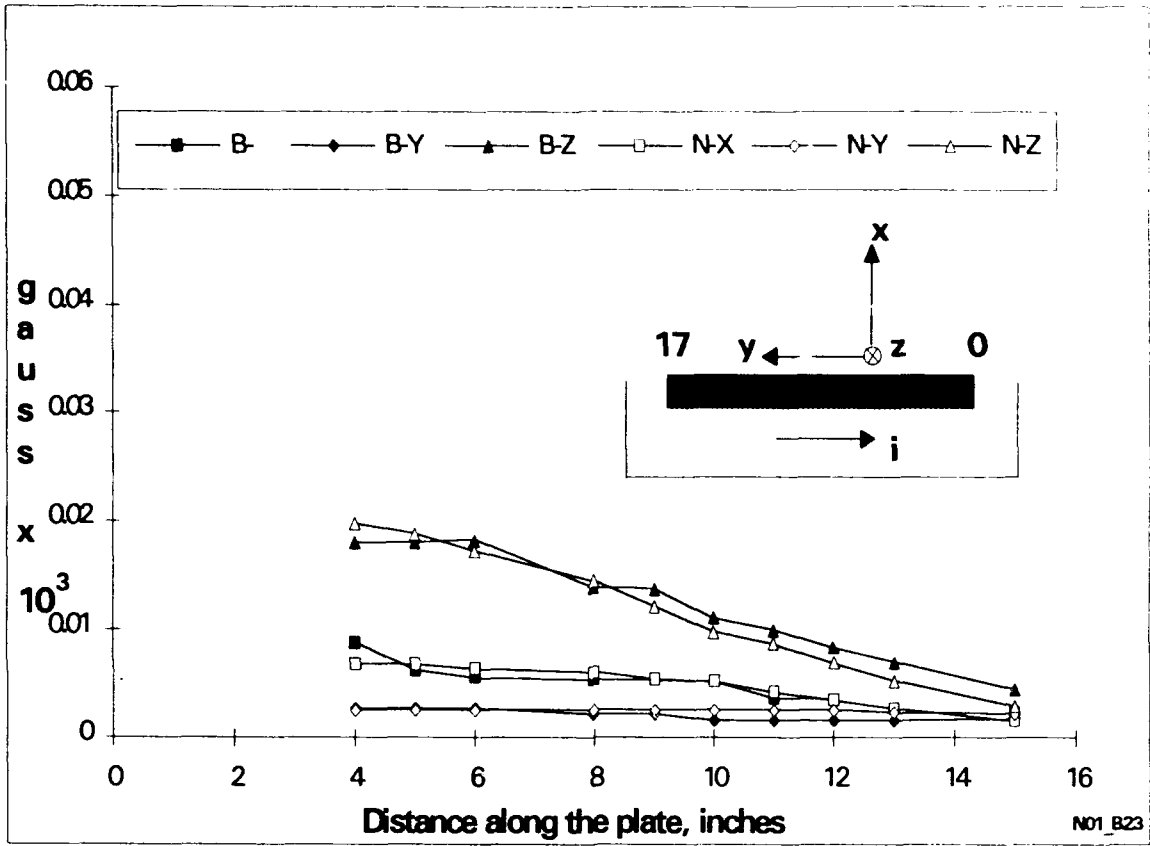
Figure 20: Counter-current flows: Magnetic field measurements on a c-304 strip with a bolt at 9 inches.
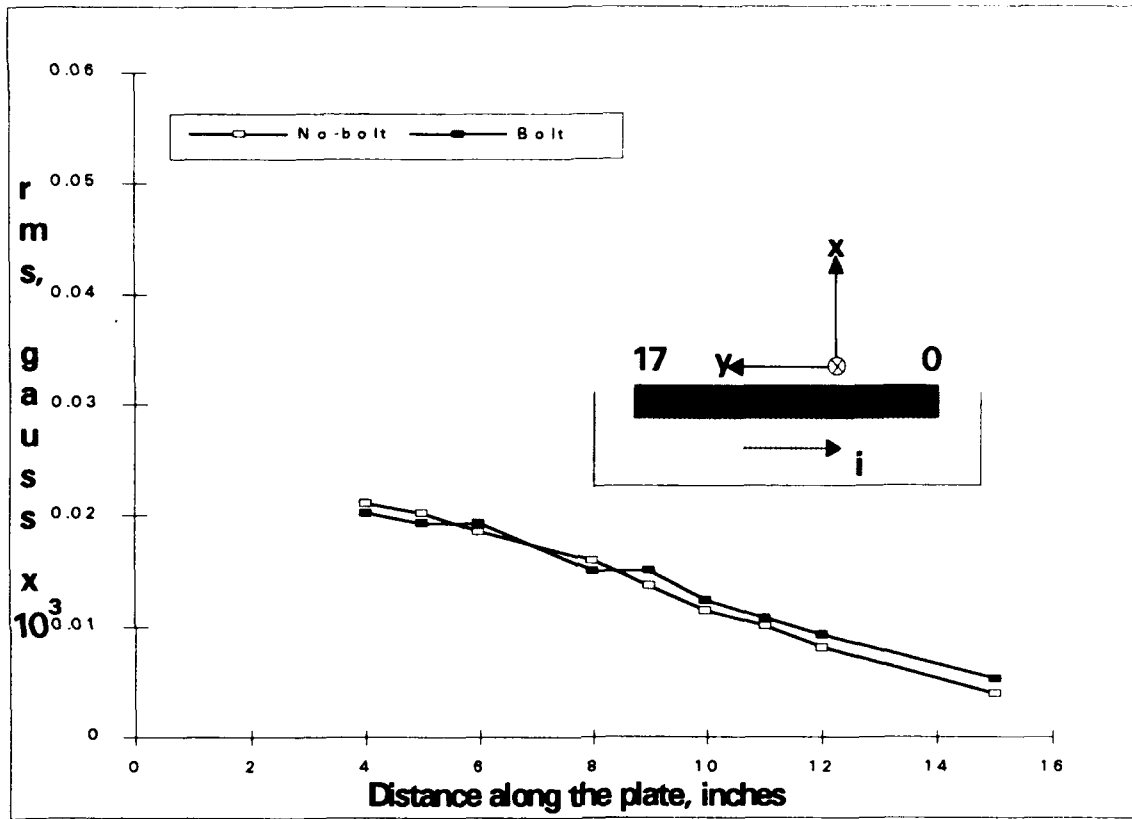
Figure 21: Counter-current flows: rms values of the magnetic field measurements shown in Figure 20.

No-Site

+I

Electronic

total

Ionic

- I

Site

+I

Electronic

total

- I
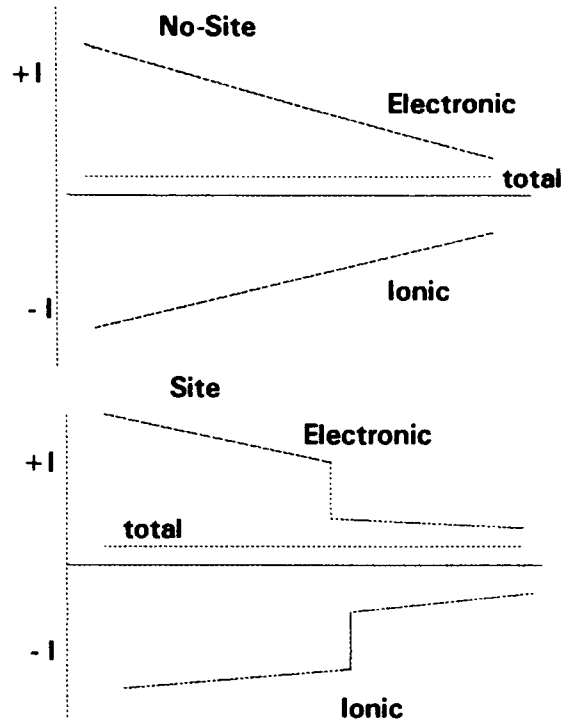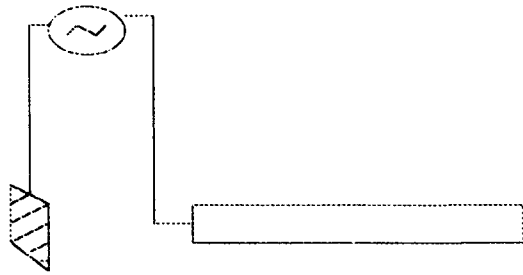
Ionic

NO1_B26

Figure 22: Schematic of the situation with counter-current flows showing the individual ionic, electronic and net total components for magnetic field measurements.
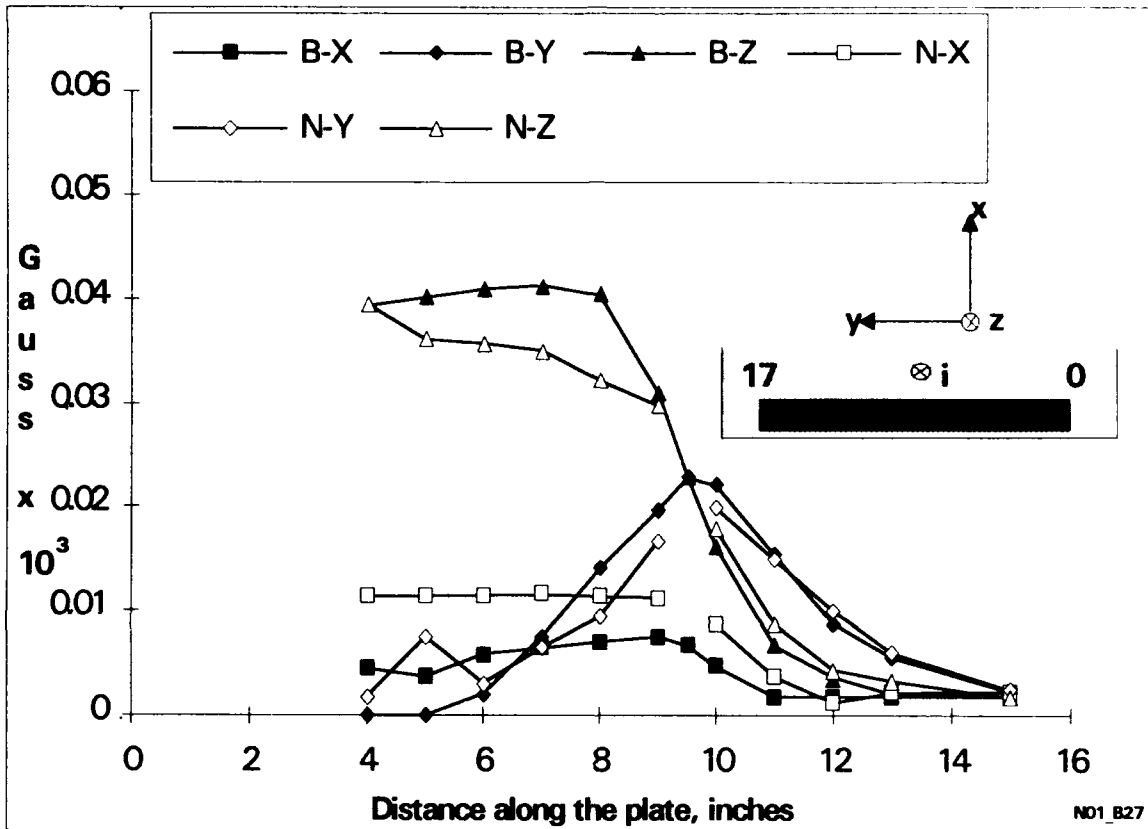
Figure 23: Perpendicular current flows: Magnetic field measurements on a c-304 strip with a bolt at 9 inches.
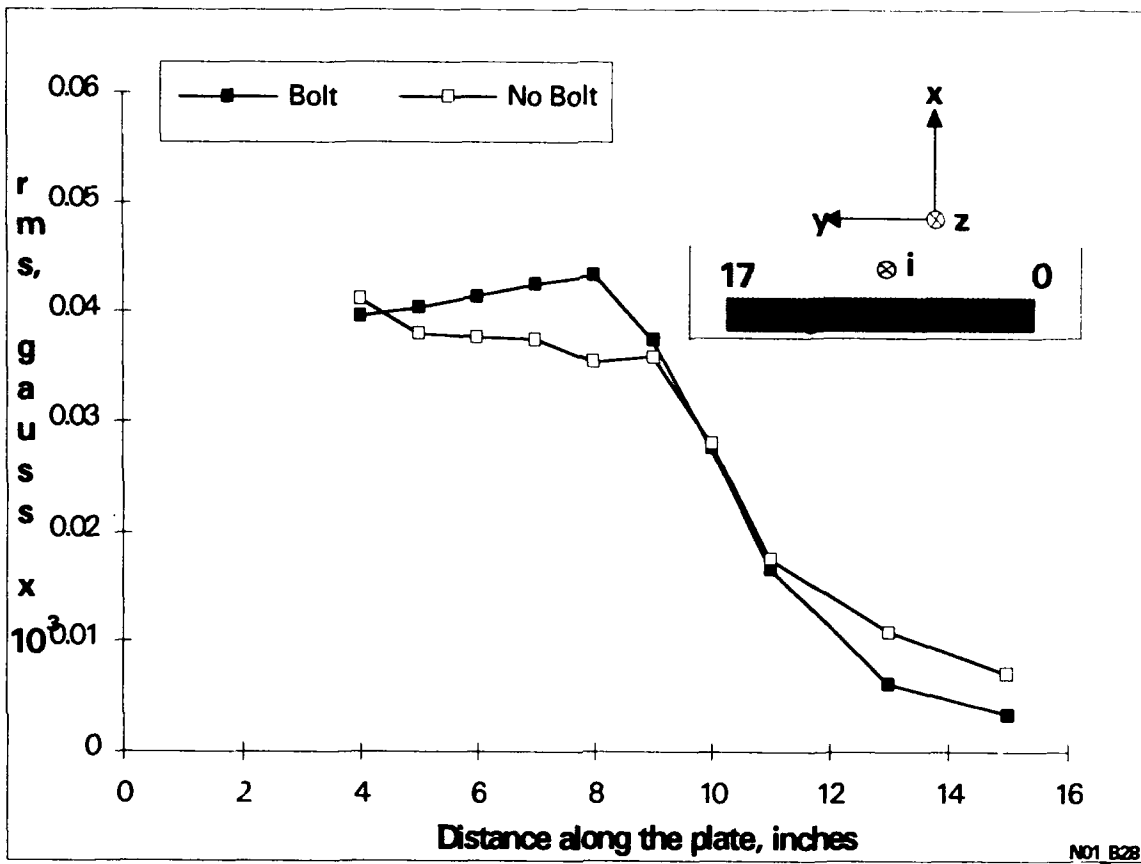
Figure 24: Perpendicular current flows: RMS values of the magnetic field measurements
shown in Figure 23.
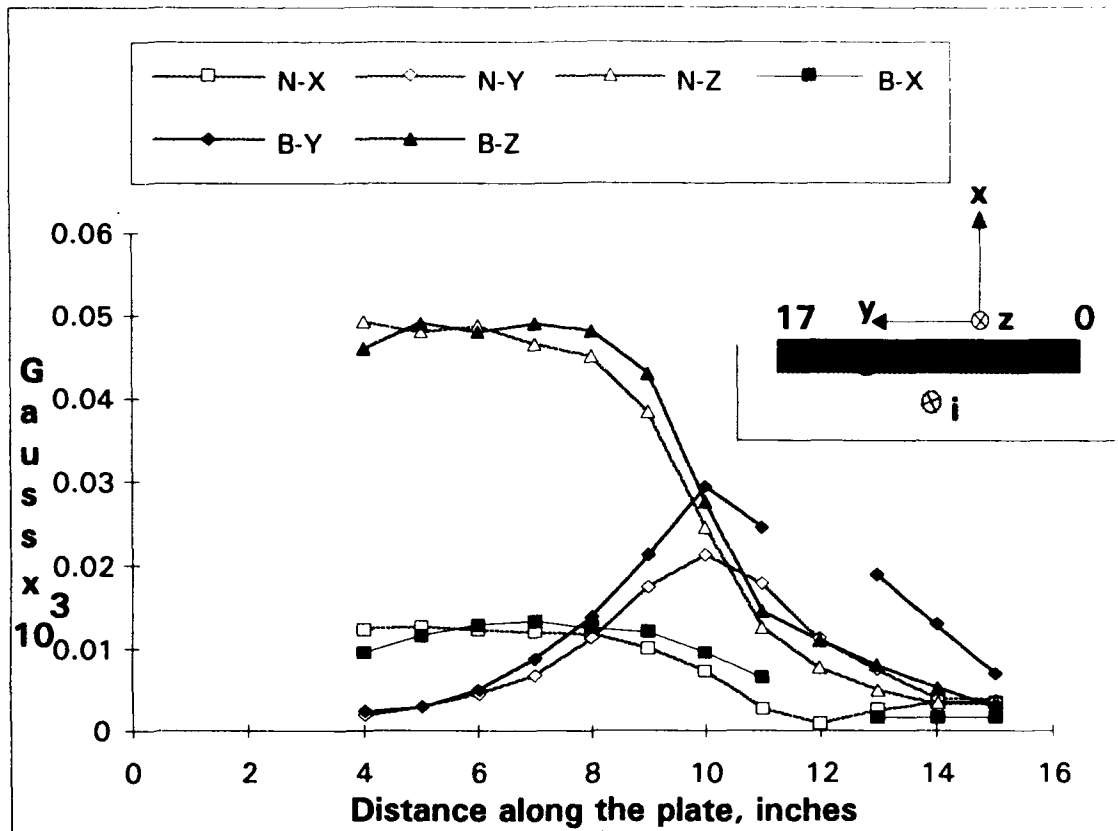
Figure 25: Perpendicular current flows: Magnetic field measurements on a c-304 metal strip with a bolt at 9 inches.
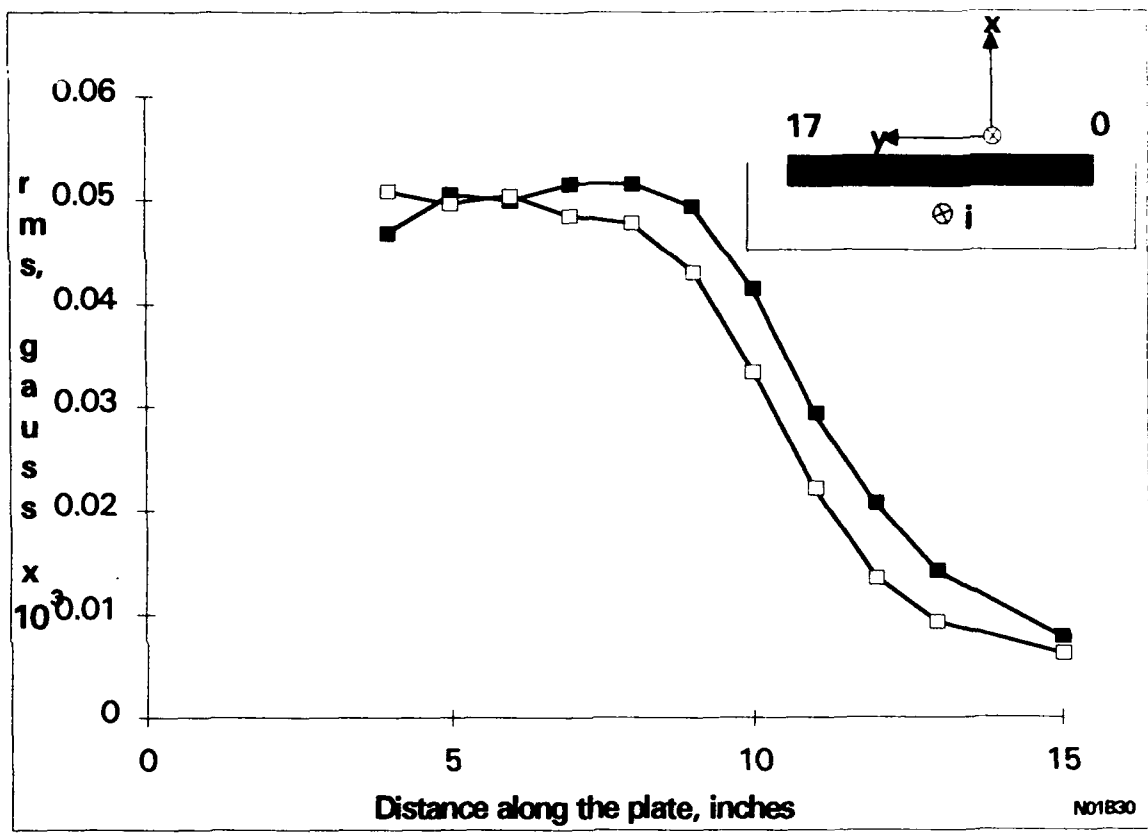
Figure 26: Perpendicular current flows: Magnetic field measurements on a c-304 strip
with a bolt at 9 inches.
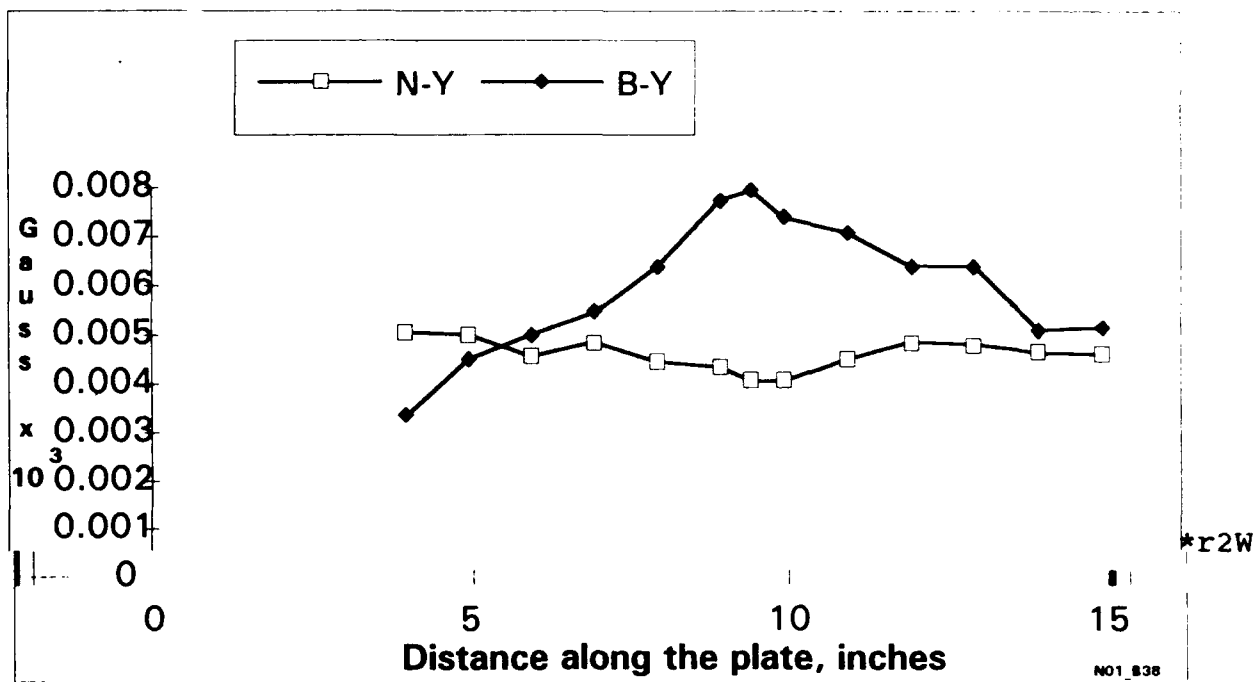
Figure 27: Magnetic field measurements over crevice sites formed by o-rings on a c-304 metal strip. For comparison, data from a plate with no crevices is also shown.
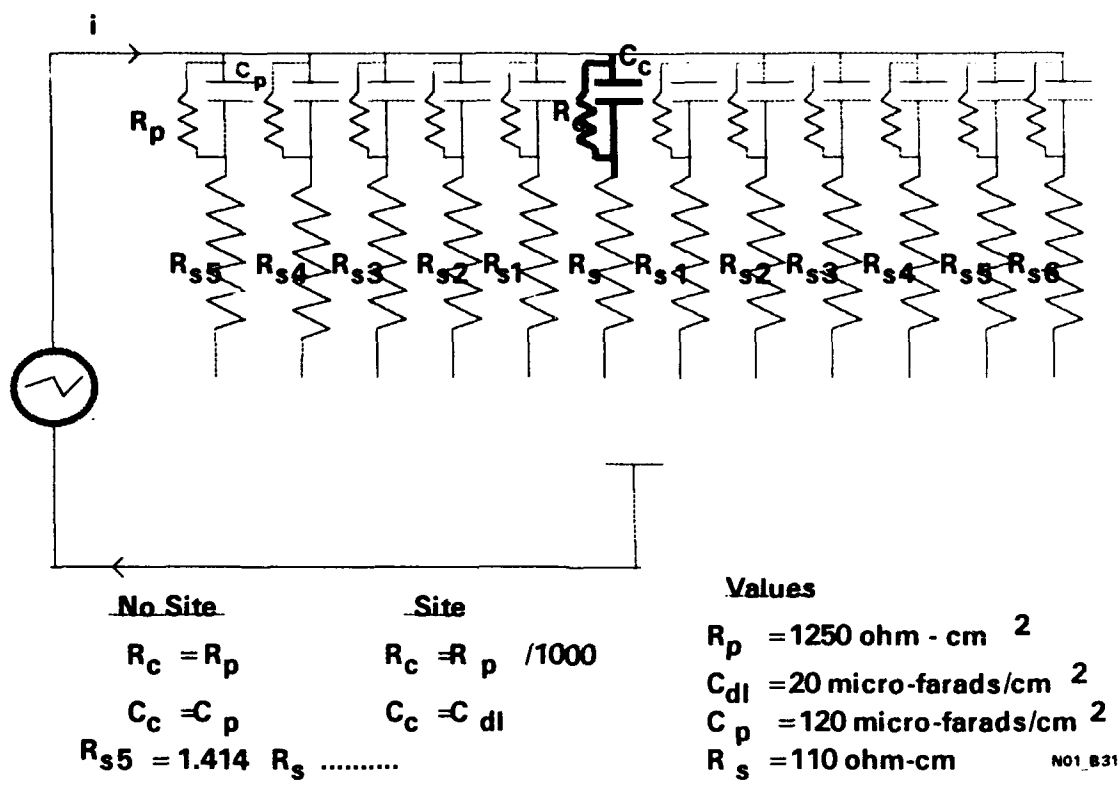
Figure 28: Equivalent analog circuit for the metal strip with the return electrode at the middle such that the leaking current flows perpendicularly to the plate.
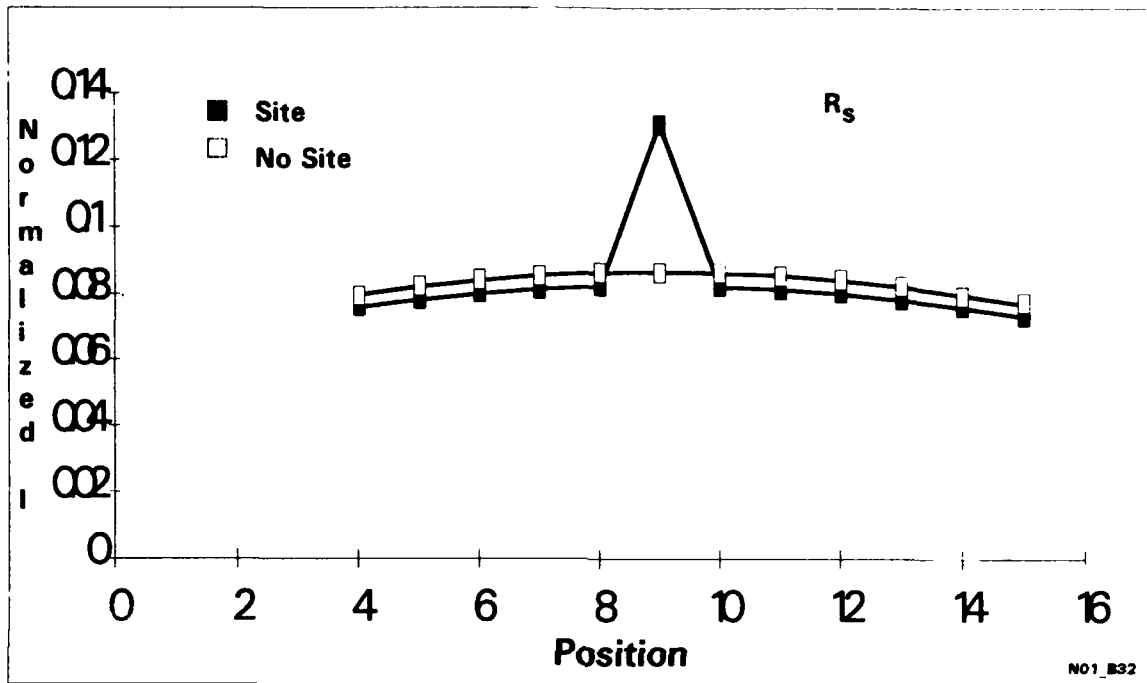
Figure 30: Model calculations with one return electrode placed closer to the crevice site. The solution resistance, R_S = 110 ohm-cm.
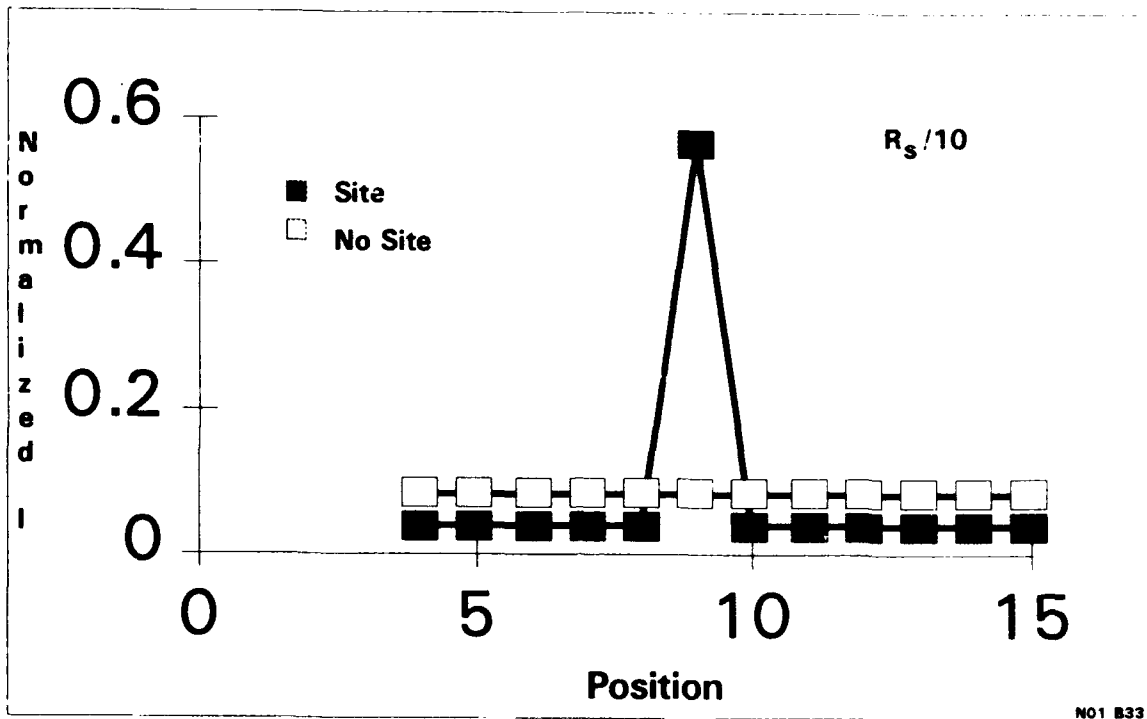
Figure 31: Model calculations showing the effect of solution resistance on signal from crevice site. Solution resistance, $R_S = 11$ ohm-cm.
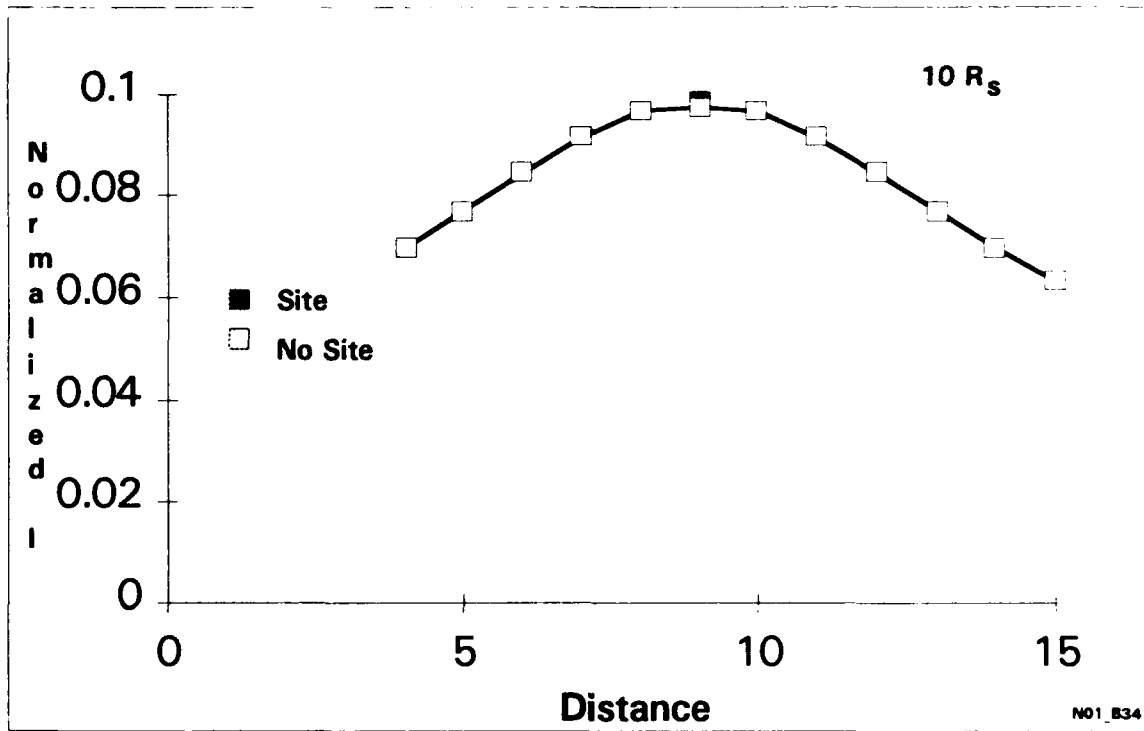
Figure 32: Model calculations showing the effect of solution resistance on the signal from crevice sites. Solution resistance, R_S = 1100 ohm-cm.

No Site

$R_c = R_p$

$C_c = C_p$

Site

$R_c = R_p/1000$

$C_c = C_{dl}$

Values

$R_p = 1250$ ohm - cm^2

$C_{dl} = 20$ micro-farads/cm^2

$C_p = 120$ micro-farads/cm^2

$R_s = 110$ ohm-cm

N01_B36
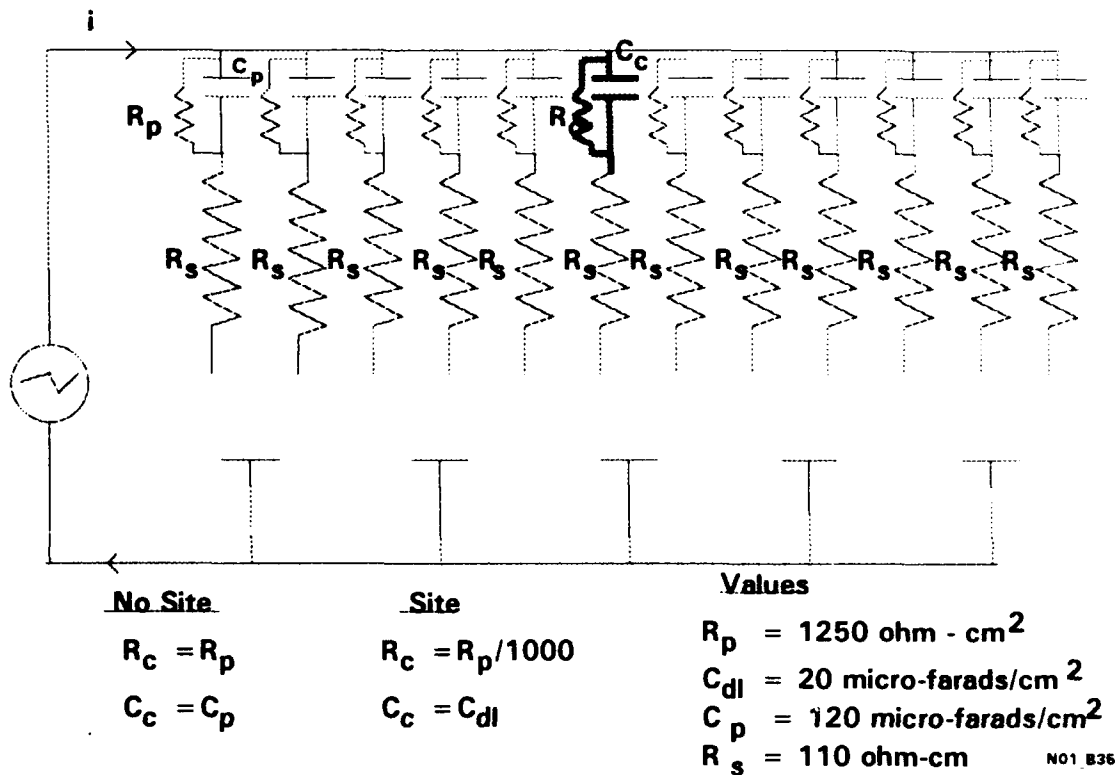
Figure 32: Equivalent analog circuit used for the calculations for five-return electrode setup.
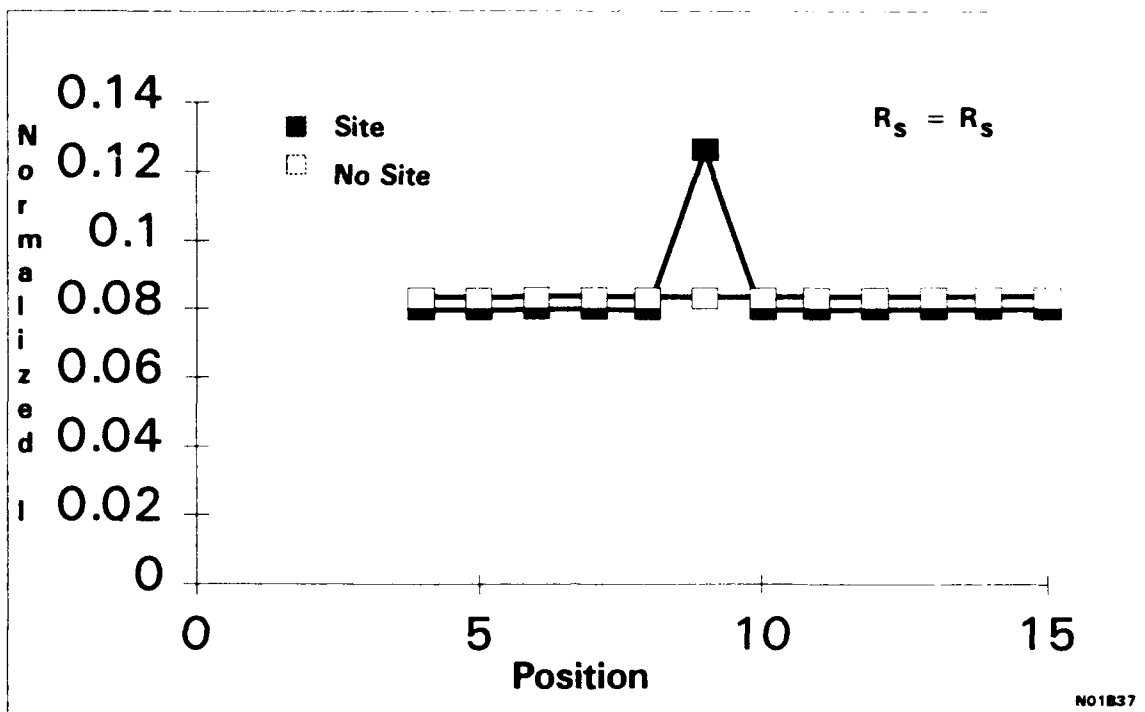
Figure 33: Model calculations with five return electrodes.
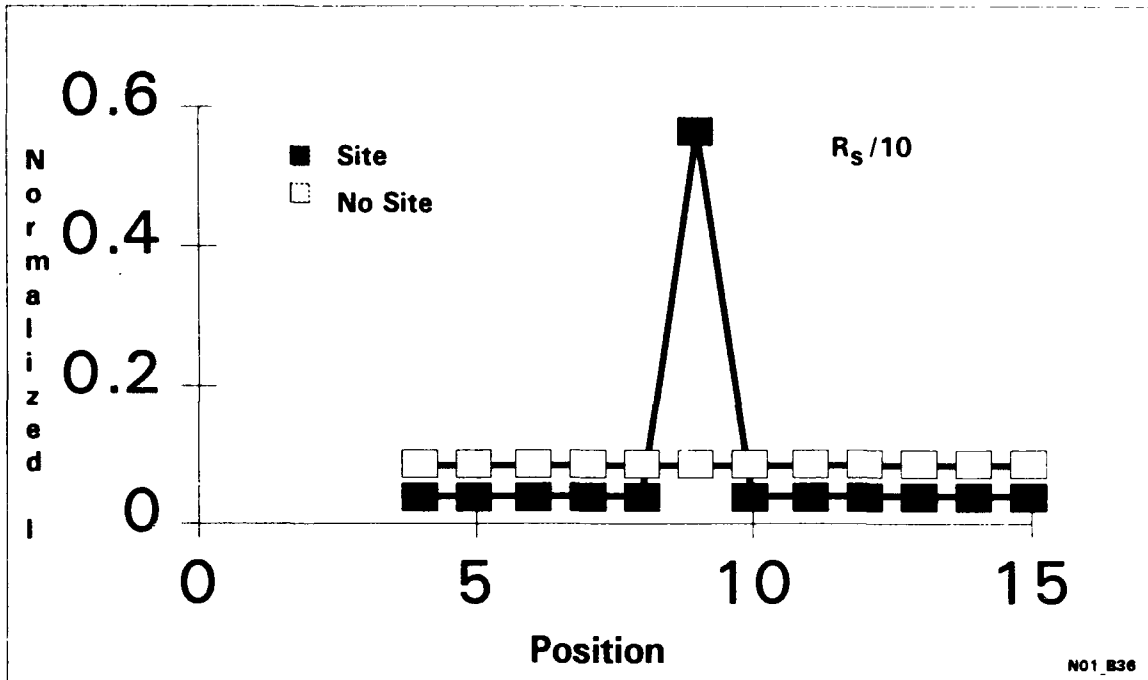
Figure 34: Model calculations with five return electrodes.
Solution resistance, R_s = 11 ohm-cm.